Detectability of Breast Tumor by a Hand-held Impulse-Radar Detector: Performance Evaluation and Pilot Clinical Study

Takamaro Kikkawa

Research Institute for Nanodevice and Bio Systems
Hiroshima University

1-4-2 Kagamiyama, Higashi-hiroshima, Hiroshima, 739-8527 Japan

E-mail: kikkawat@hiroshima-u.ac.jp

Outline

1. Introduction
2. Dielectric properties of cancer
3. Breast cancer detection system
4. Clinical examination
5. Conclusion

Breast Cancer Tissues

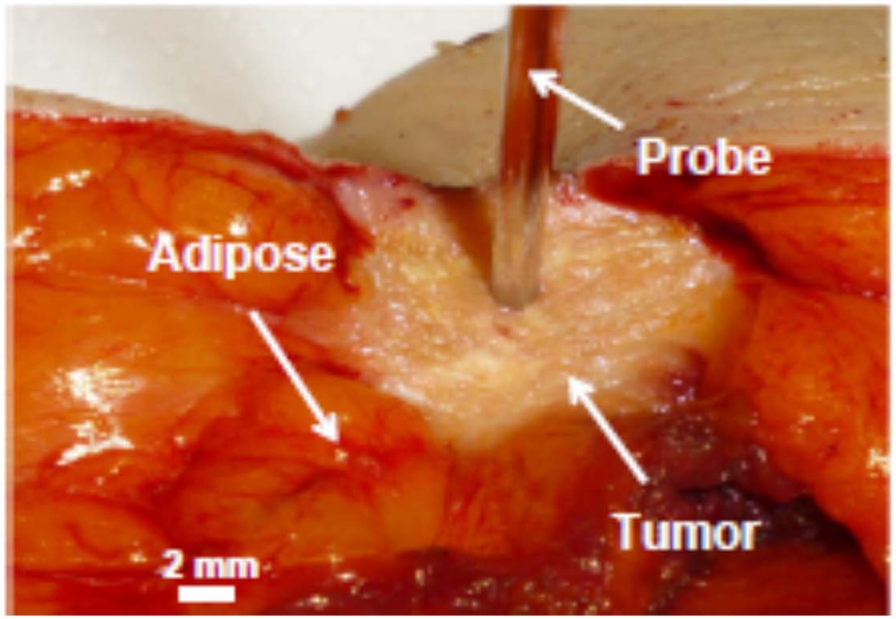

- Photograph of breast cancer tissue excised from patient
- Measurement carried out with open-ended coaxial probe (2.2mm outer diameter) on tumor region of ill-defined and grayish-white on the cut surface

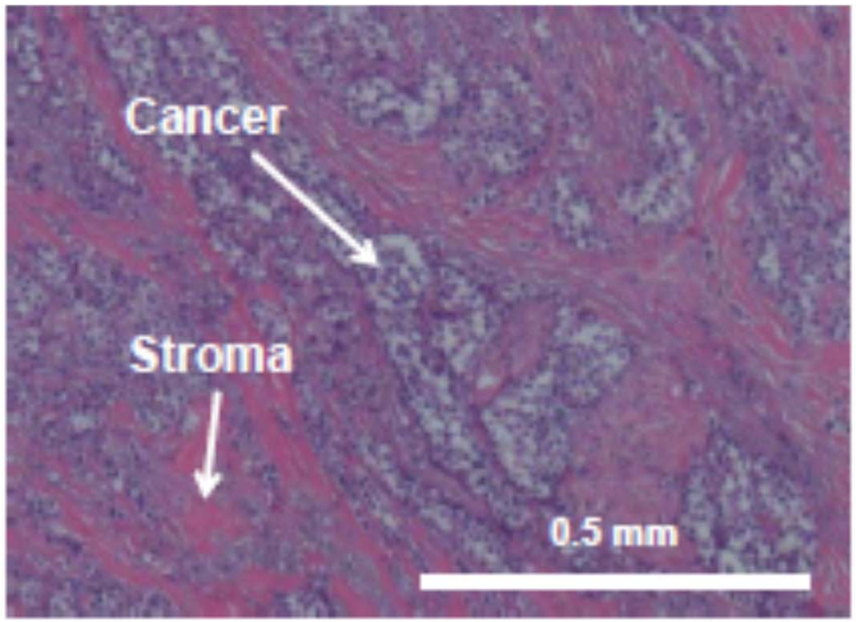

- Digital photomicrograph image of malignant tumor tissue with hematoxylin-eosin staining
- Tumor tissue is not fully occupied by the cancer cells (gray) but cancer cells are distributed locally in the stroma cells (red)

T. Sugitani *et al.*, Applied Physics Letters 104, 2014, pp. 253702-1-5.

Measurement of Permittivity of Excised Tumor Tissue

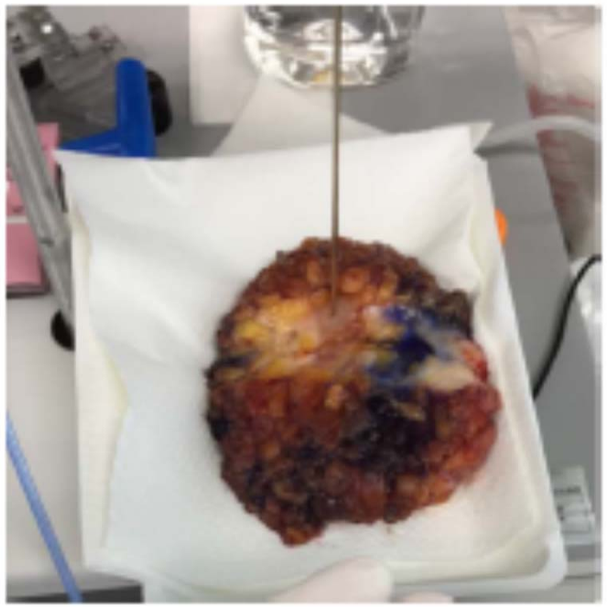

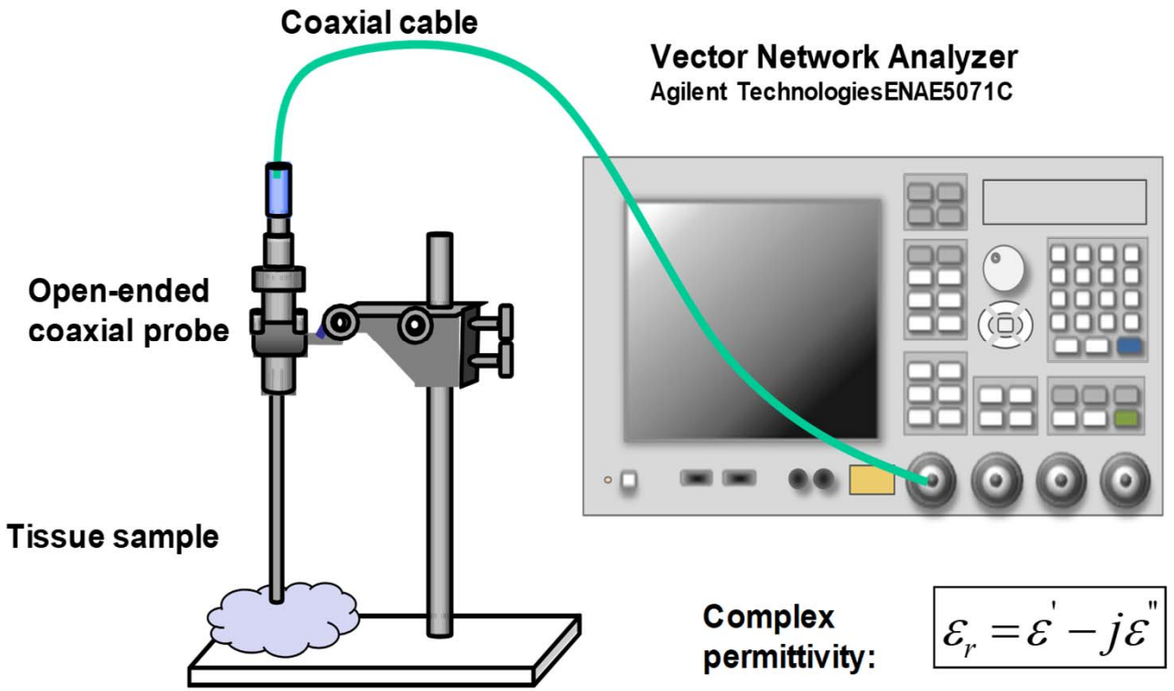

- Dielectric properties of breast tissues measured at 0.5–20 GHz using Agilent E5071C vector network analyzer (VNA) and open-ended coaxial probe of Agilent 85070 dielectric probe kit
- Probe aperture outer diameter = 2.2mm, length = 200mm
- VNA calibrated at reference plane of coaxial probe tip using calibration standards (e.g., open circuit in air, short circuit with a metal, and load in liquids)

T. Sugitani *et al.*, Applied Physics Letters 104, 2014, pp. 253702-1-5.

Dielectric Properties of Breast Cancer

- Permittivity and conductivity of breast cancer tissues higher than those of normal breast tissues in microwave frequency band

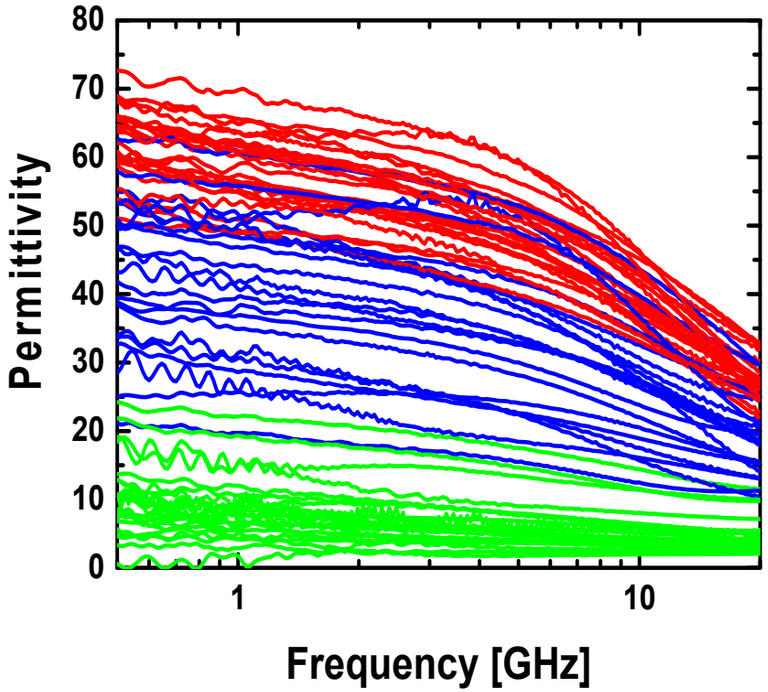

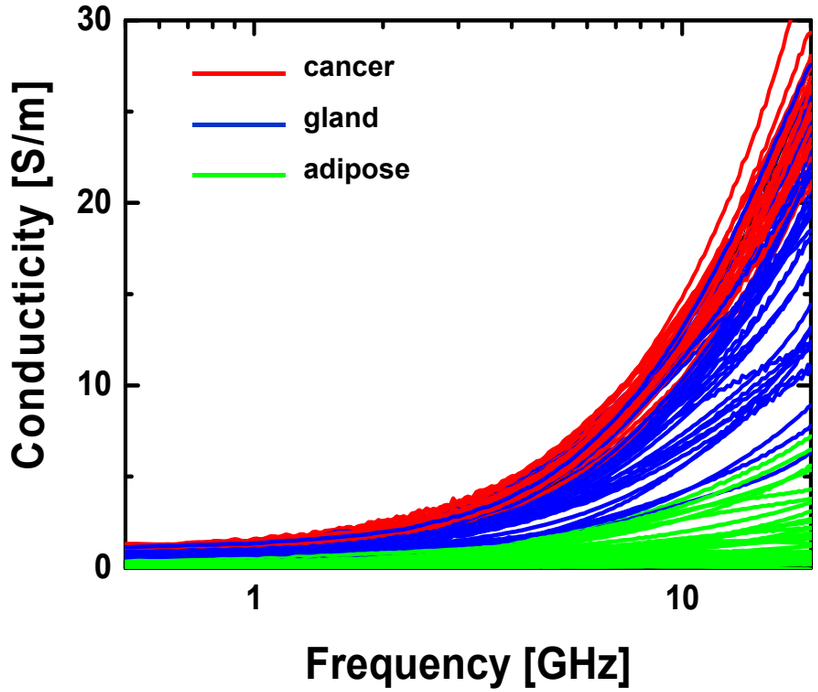

- Statistical uncertainty observed in dielectric constant and conductivity between cancer and glandular tissues, as well as between glandular and adipose tissues
- Therefore difficult to statistically distinguish cancer from normal tissues

T. Sugitani *et al*., Applied Physics Letters 104, 2014, pp. 253702-1-5.

Dielectric Properties of Breast Cancer of Individual Patients

(a)

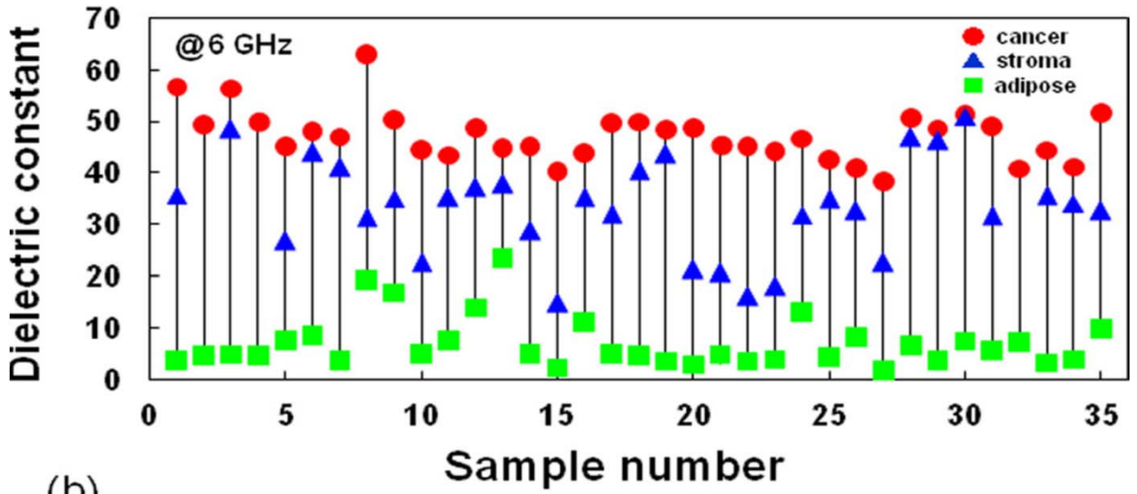

(b)

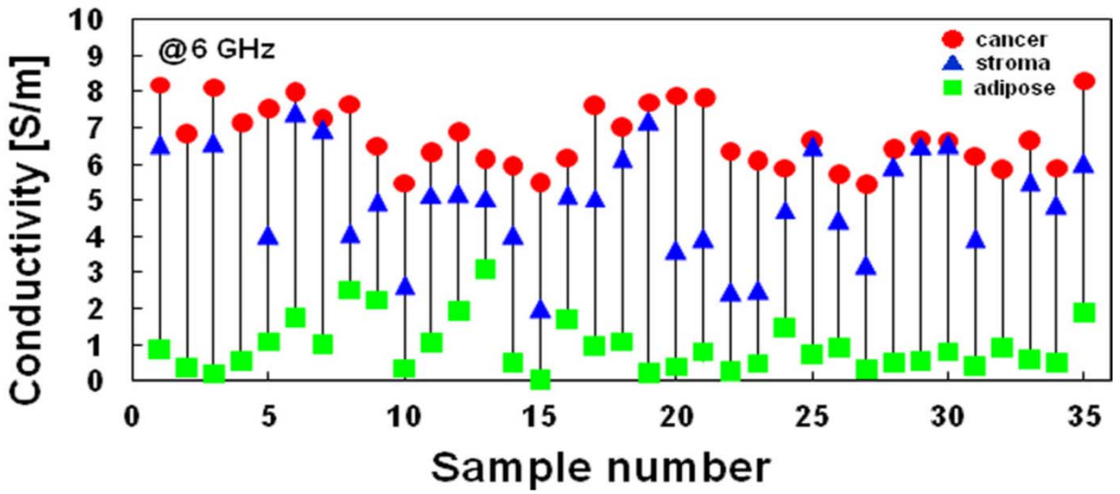

T. Sugitani *et al*., Applied Physics Letters 104, 2014, pp. 253702-1-5.

Dielectric Model of Breast Tissues
(Modified Cole-Cole Model)

- Model measurement data with modified Cole-Cole model to understand the characteristics quantitatively

$$\varepsilon^{'}(\omega) - j\varepsilon^{''}(\omega) = \varepsilon_{\infty} + \frac{\varepsilon_m - \varepsilon_{\infty}}{1 + \left(j\omega\tau_Q\right)^{1-\beta}} + \frac{\varepsilon_s - \varepsilon_m}{1 + j\omega\tau_P} - \frac{\sigma_s}{\omega\varepsilon_0} j$$

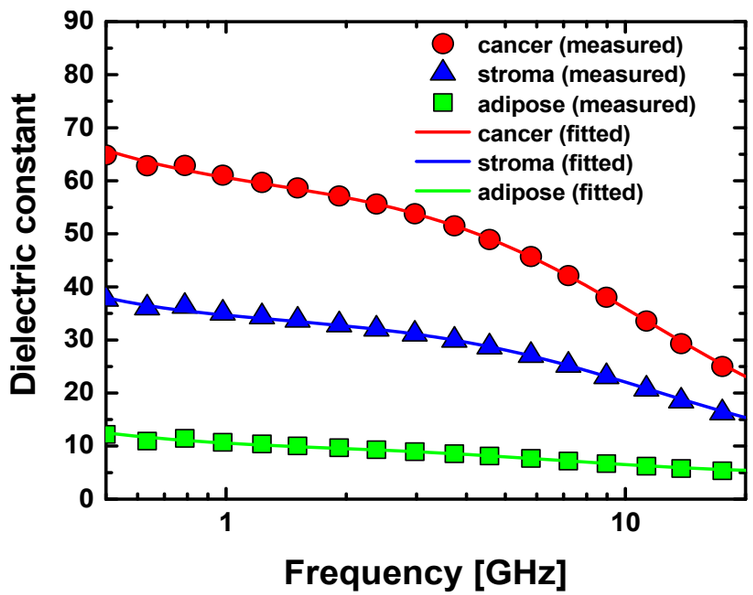

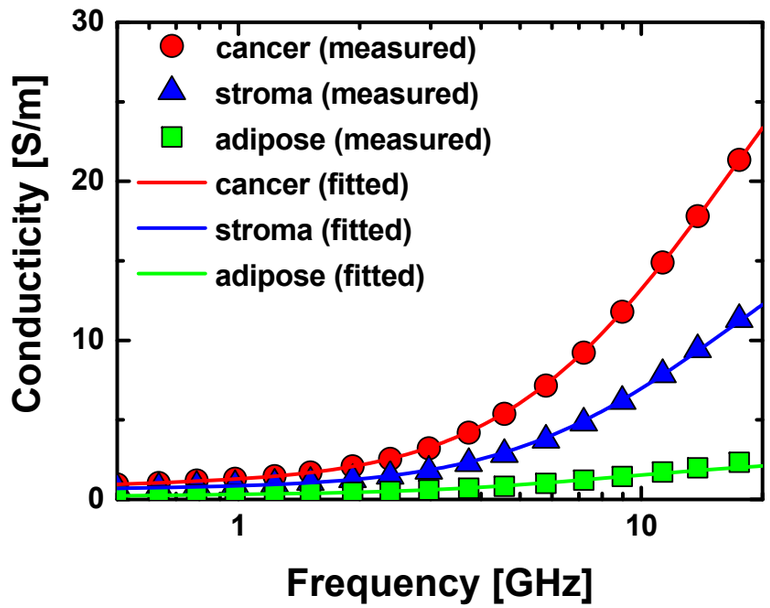

T. Sugitani *et al*., Applied Physics Letters 104, 2014, pp. 253702-1-5.

Model Parameters of Breast Tissues

Modified Cole-Cole Model

$$\varepsilon^{'}(\omega) - j\varepsilon^{''}(\omega) = \varepsilon_{\infty} + \frac{\varepsilon_m - \varepsilon_{\infty}}{1 + \left(j\omega\tau_Q\right)^{1-\beta}} + \frac{\varepsilon_s - \varepsilon_m}{1 + j\omega\tau_P} - \frac{\sigma_s}{\omega\varepsilon_0} j$$

Cancer, stroma and adipose tissues can be classified by model parameters of epsilon at medium frequency and conductivity.

Coefficients	Cancer	Stroma	Adipose
ε_∞	7.17	7.94	4.26
ε_m	59.45	33.2	9.26
ε_s	67.99	40.3	12.6
τ_P (ns)	0.212	0.23	0.164
τ_Q (ps)	13.9	13.7	18.29
β	0.11	0.074	0.0617
σ_S (S/m)	0.759	0.553	0.184

T. Sugitani *et al.*, Applied Physics Letters 107, 019902 (2015).

Microwave Imaging Systems under Development

Radar-based microwave imaging system（Bristol University, UK)

3D tomography microwave imaging system（Dartmouth University, USA)

A. Modiri *et al*., Medical Physics 44(12), pp. 3446-458, 2017.

Principle of Radar-based Detection

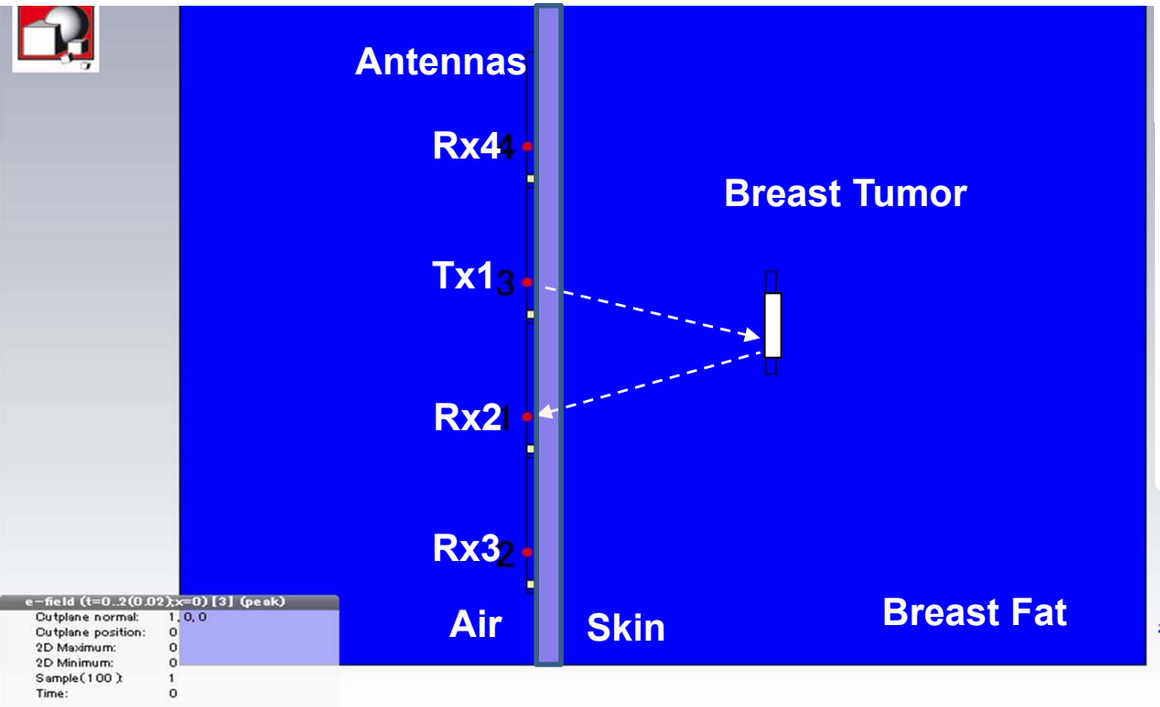

Received Waveform

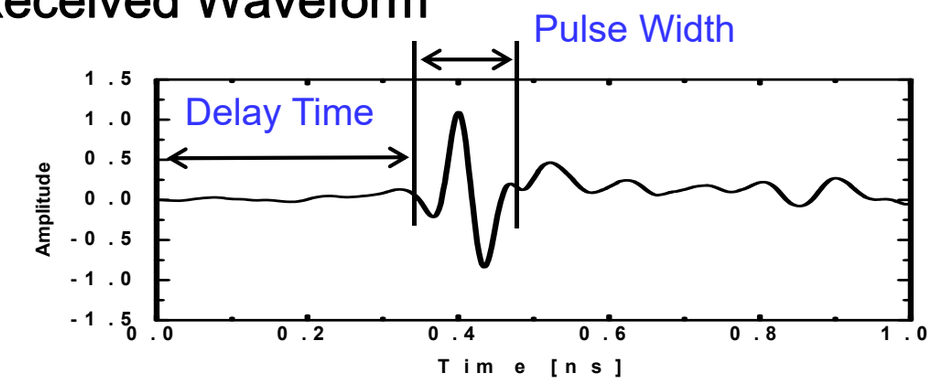

Time-to-Distance Conversion: Ellipsoidal Curves

$$I(P) = \sum_{i=1}^{Emitter} \sum_{j=1}^{Detector} \int S_{i,j}\left(\frac{\sqrt{\varepsilon_r}(L_1 + L_2)}{c}\right)$$

I(P): Energy of a certain point *P*
$S_{i,j}$: Signal from j to j
L_1, L_2 : the distance between the point P and antennas.
ε_r : the assumed relative permittivity of the breast.
C: the speed of light.

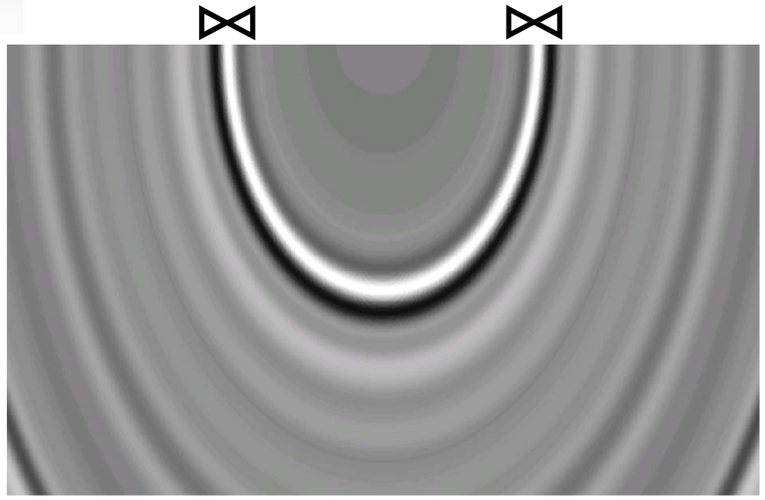

Breast Cancer Detection System Using CMOS Integrated Circuits

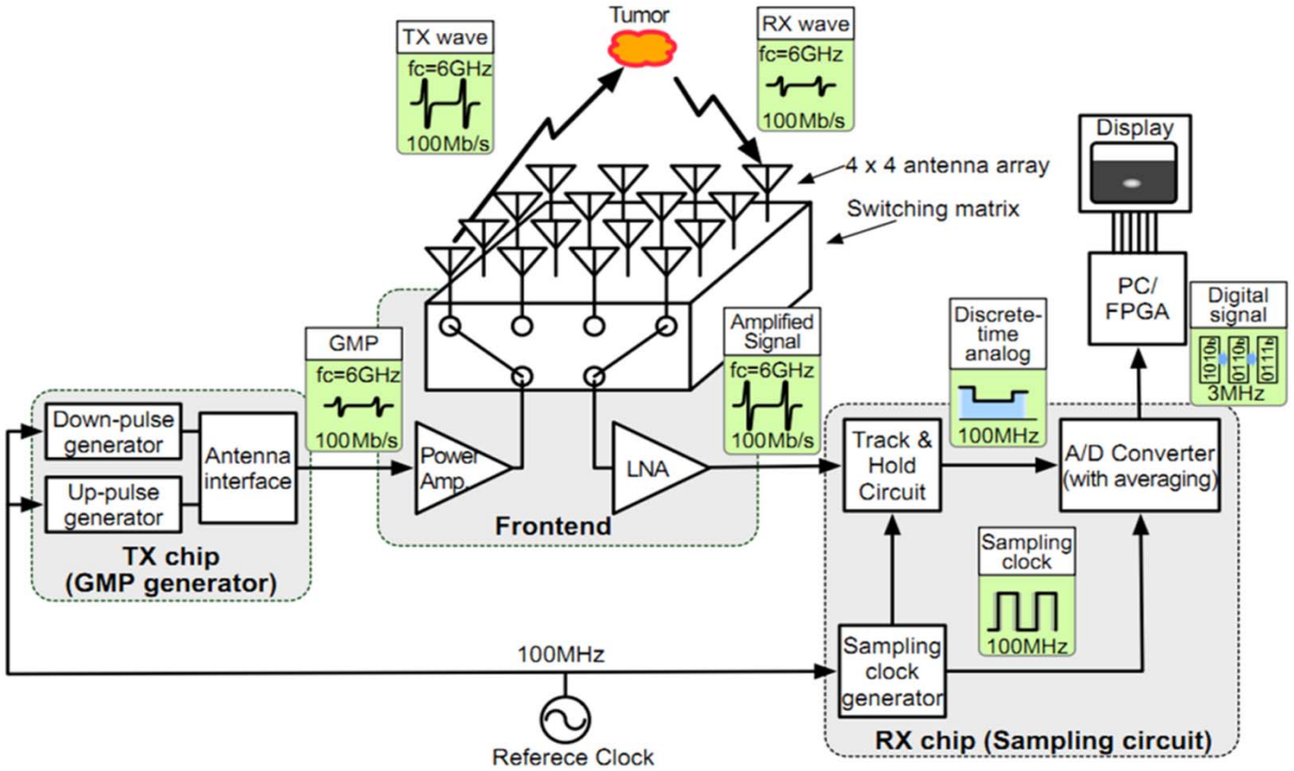

Tx chip: Generate up/ down slopes of input clock and data digital pulses to form Gaussian monocycle pulse (GMP)

Switching Matrix: Change the operating antenna pair, single pole eight throw (1P8T) switching matrix circuit

Rx chip : Record scattered signal from the cancer, high-speed equivalent time sampling circuit

Block Diagram of Breast Cancer Detection

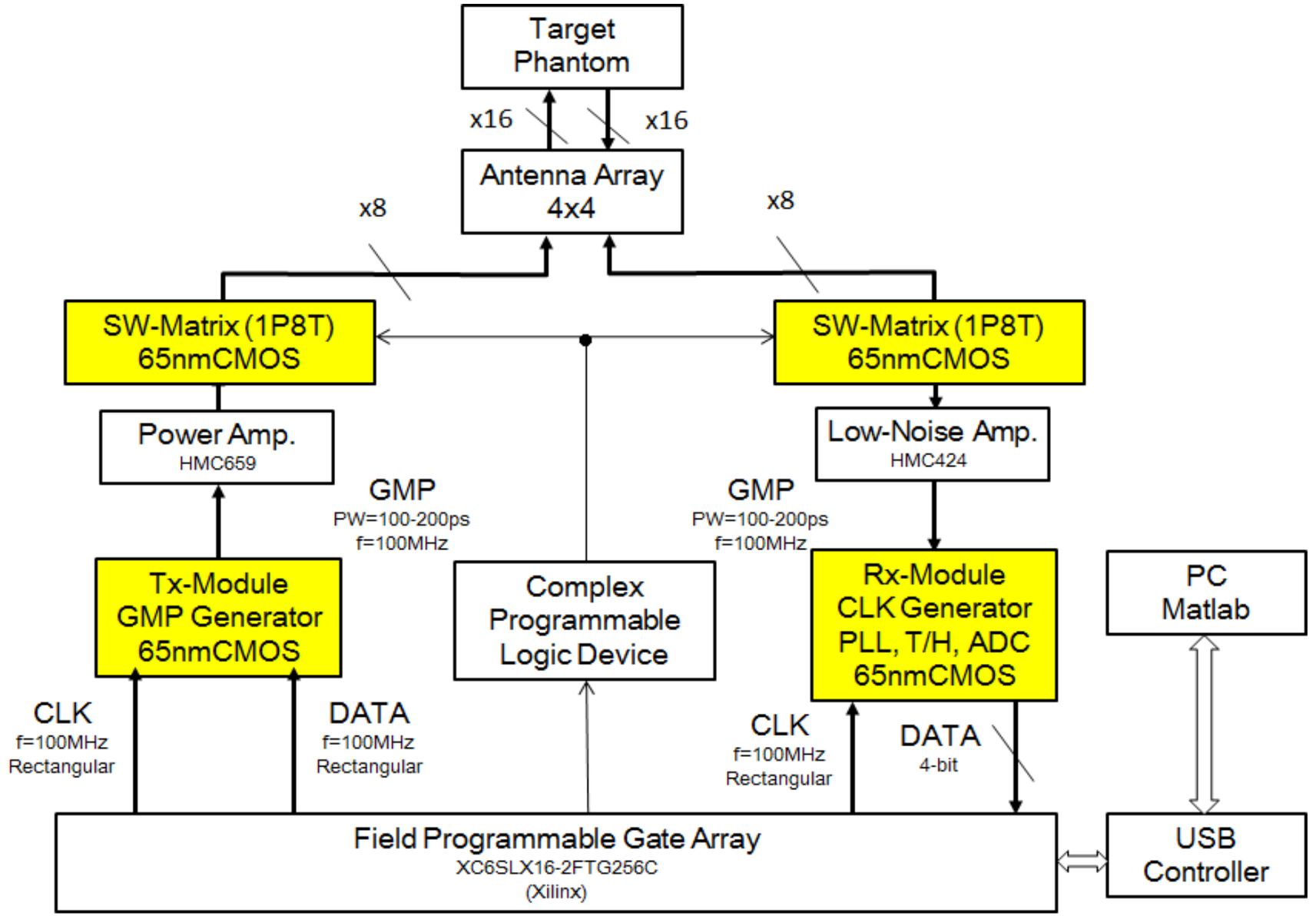

H. Song *et al*., IEEE Access, (Volume:3) Page(s):2111 – 2121, 29 Oct., 2015

Prototype of Breast Cancer Detector

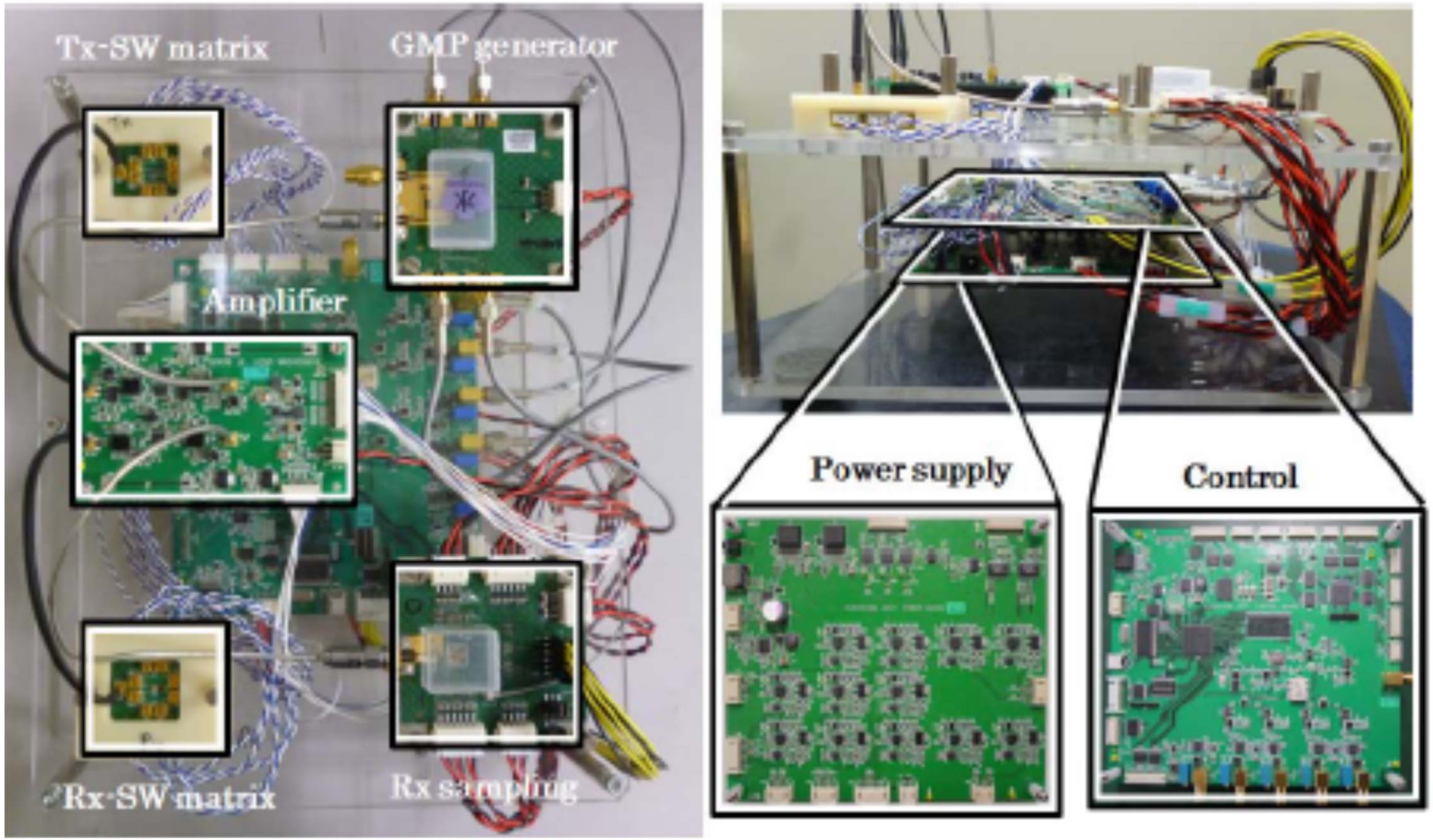

H. Song *et al*., IEEE Access, (Volume:3) Page(s):2111 – 2121, 29 Oct., 2015

GMP Generator and Transmitter Module

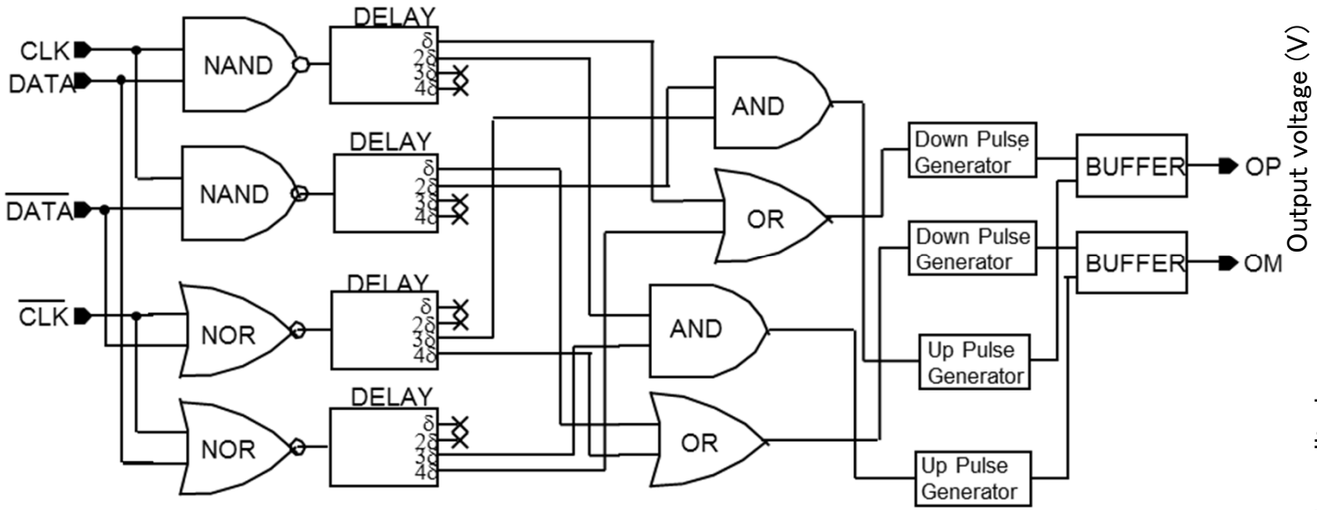

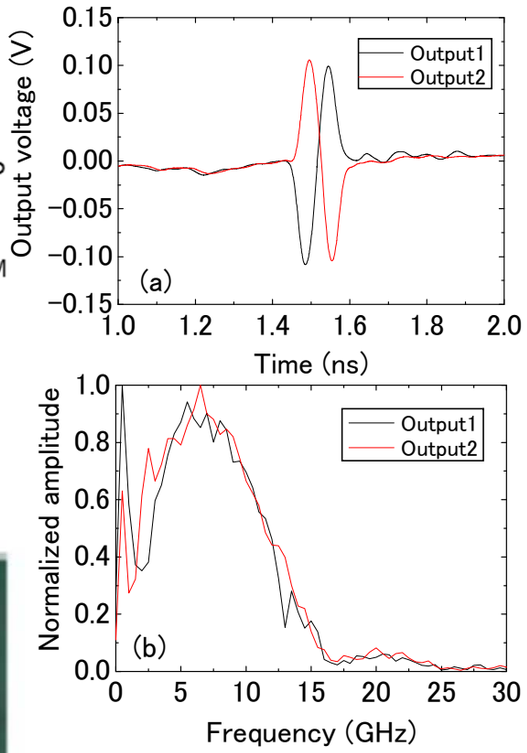

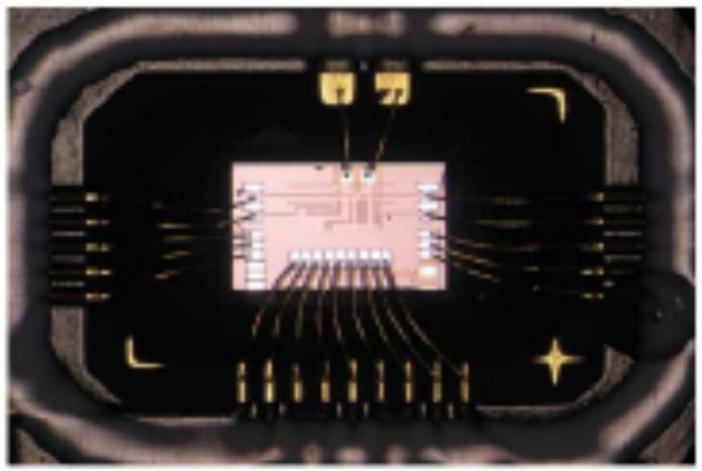

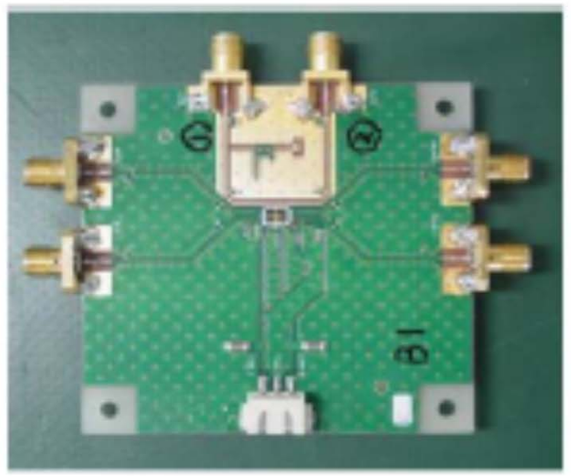

Pulse Width: 170ps
Center Frequency: 6GHz

H. Song *et al*., IEEE Access, (Volume:3) Page(s):2111 – 2121, 29 Oct., 2015

GMP Generator with Wave Correction

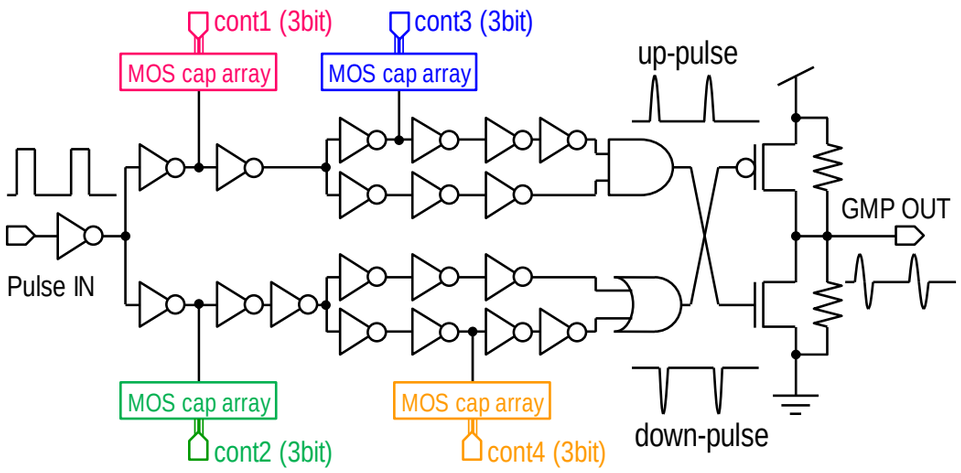

【cont1 and cont2】
Timing of combining the up-/down-pulse can be adjusted

【cont3 and cont4】
Amplitudes on the up/down side can be adjusted

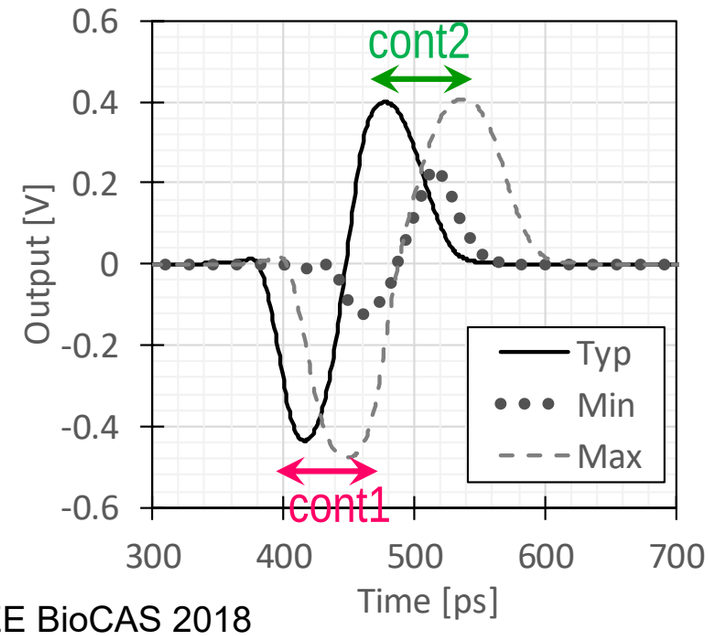

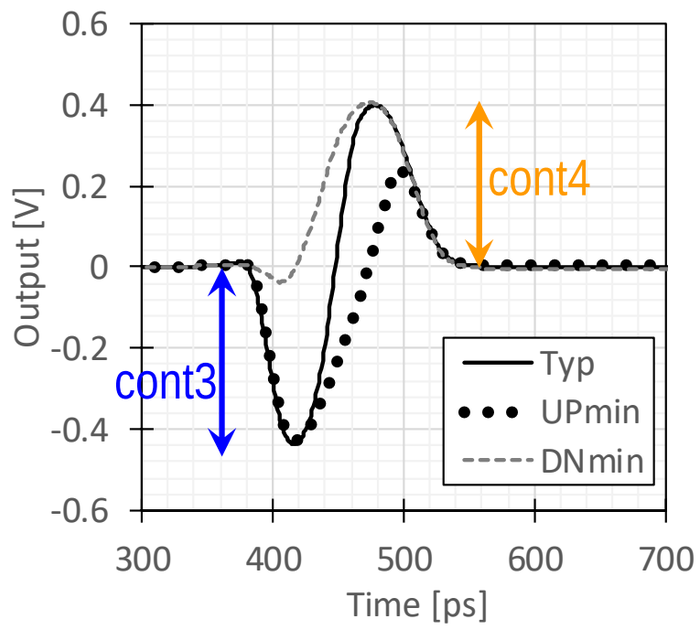

Y. Masui *et al.*, IEEE BioCAS 2018

Principle of Equivalent-Time Sampling

- Sampling clock generator determines sampling timing which is synchronized with GMP input signal with delay time (ΔT)
- T/H circuit down-converts the GMP input signal to lower frequency intermediate signal (V_{LF})
- Enables a high-speed and low power consumption sampling circuits

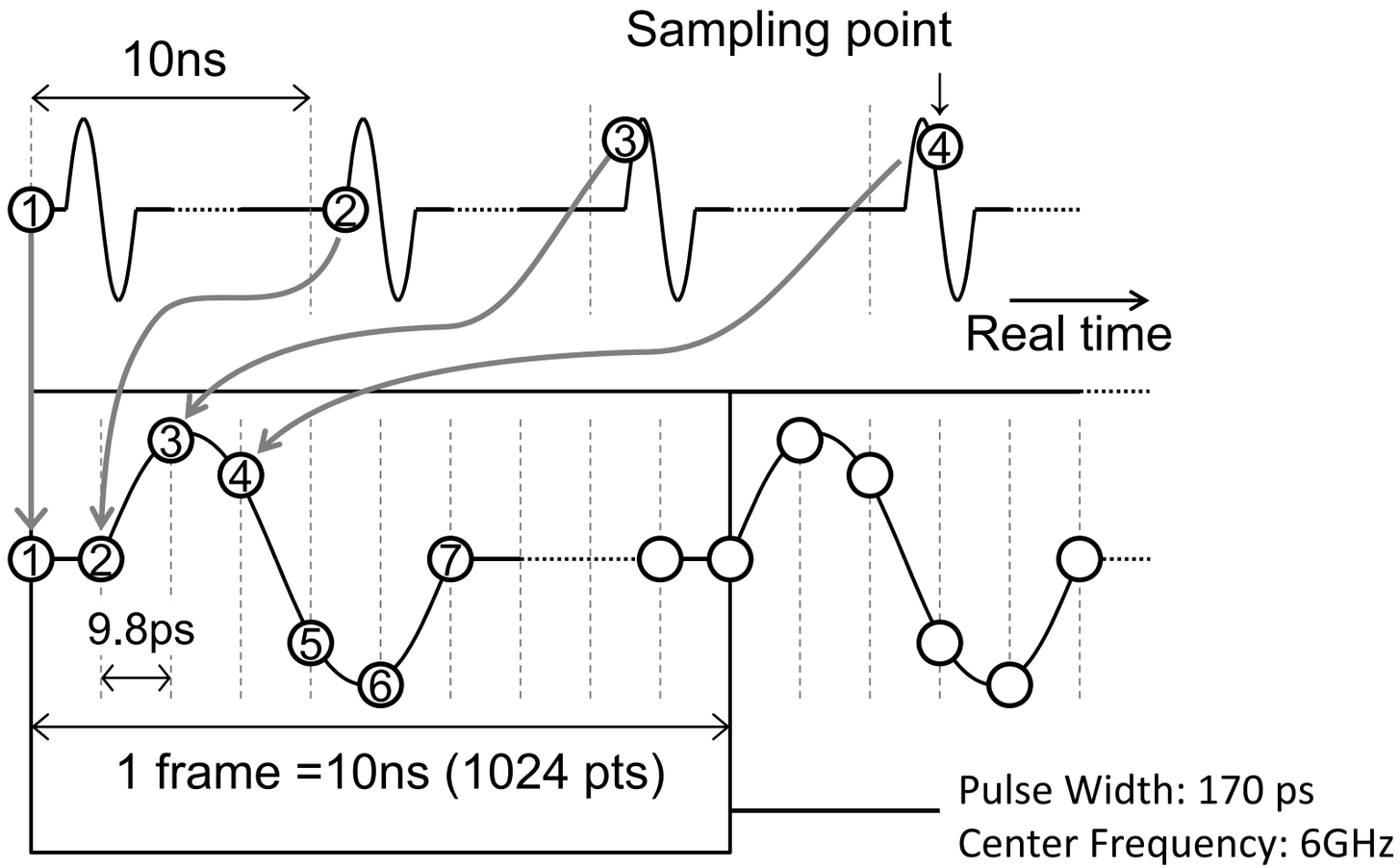

Y. Masui *et al*., IEEE BioCAS 2018

GMP Equivalent Time Sampling

Rx chip

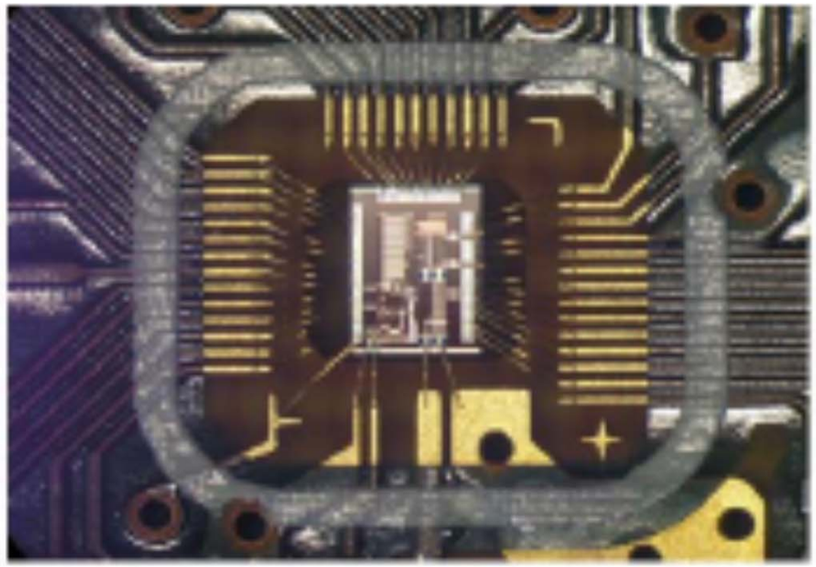

Rx module

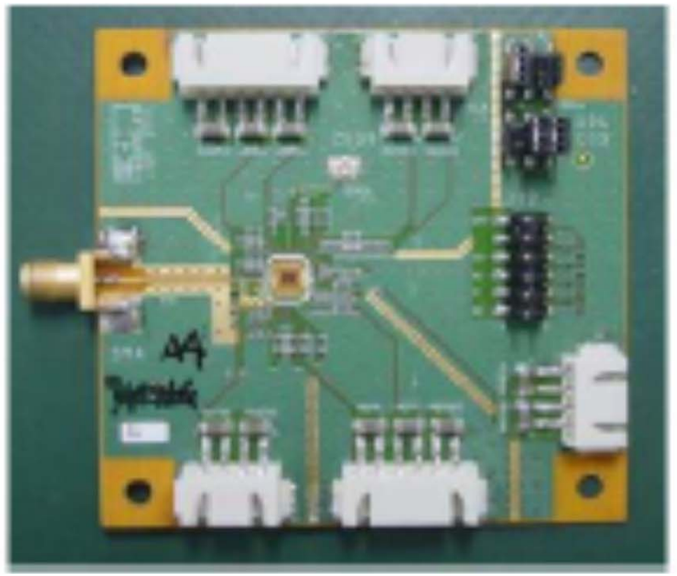

100MSps ADC + Equivalent-time sampling
⇒ 102.4 GHz sampling

H. Song *et al*., IEEE Access, (Volume:3) Page(s):2111 – 2121, 29 Oct., 2015

GMP Equivalent Time Sampling Circuits

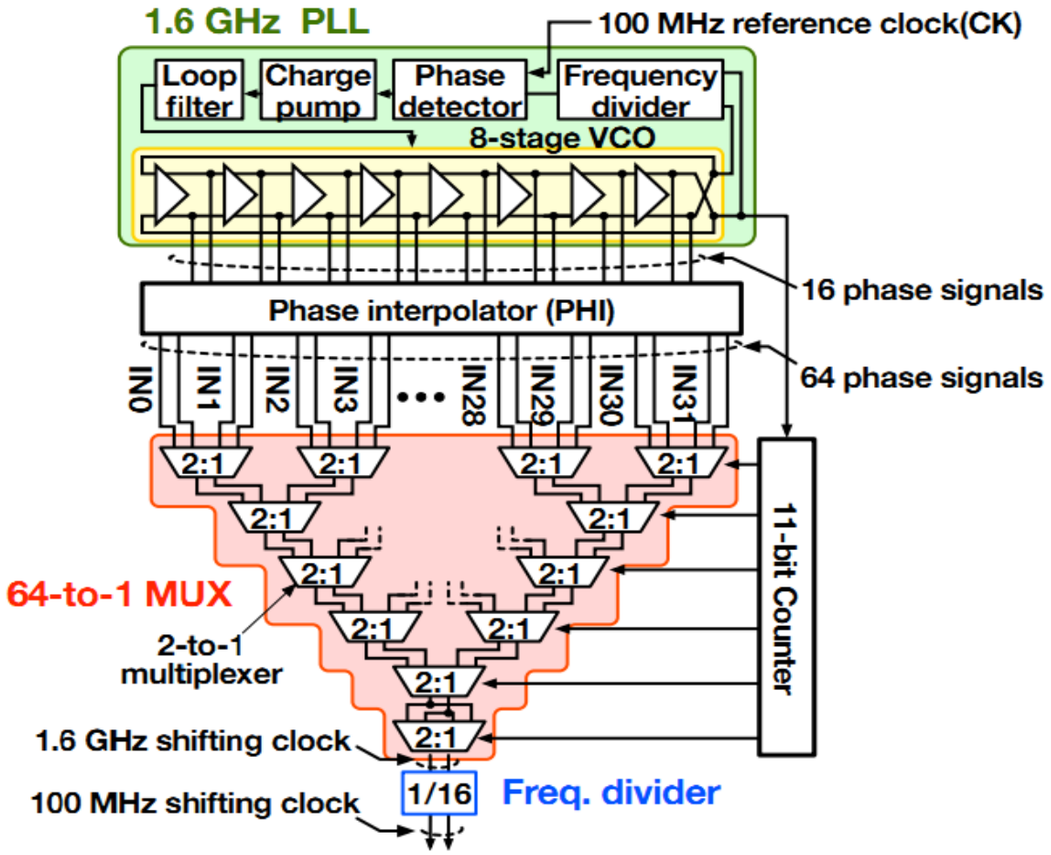

Timing diagram

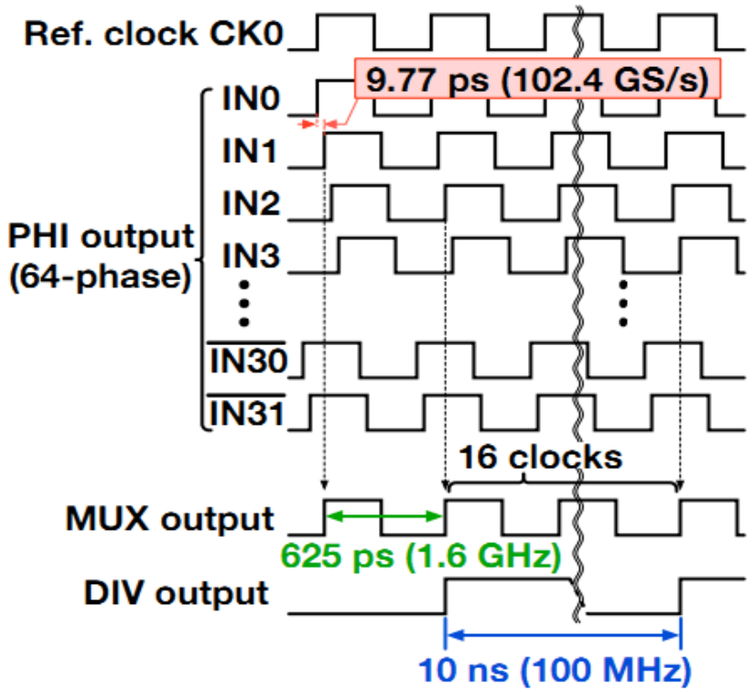

PLL generates 16-phase 1.6 GHz clock. (A phase interval is 39 ps)
PHI interpolate the phase interval. (A phase interval is 9.77 ps)
MUX selects 1 phase so that 1.6 GHz sliding clock is generated.
1/16 DIV divides frequency so that 100 MHz sliding clock is generated.
102.4 GS/s equivalent time sampling can be realized.

A. Toya *et al*., Japanese Journal of Applied Physics 52 (2013) 04CE07 (6 pages)

SP8T Switching Matrix

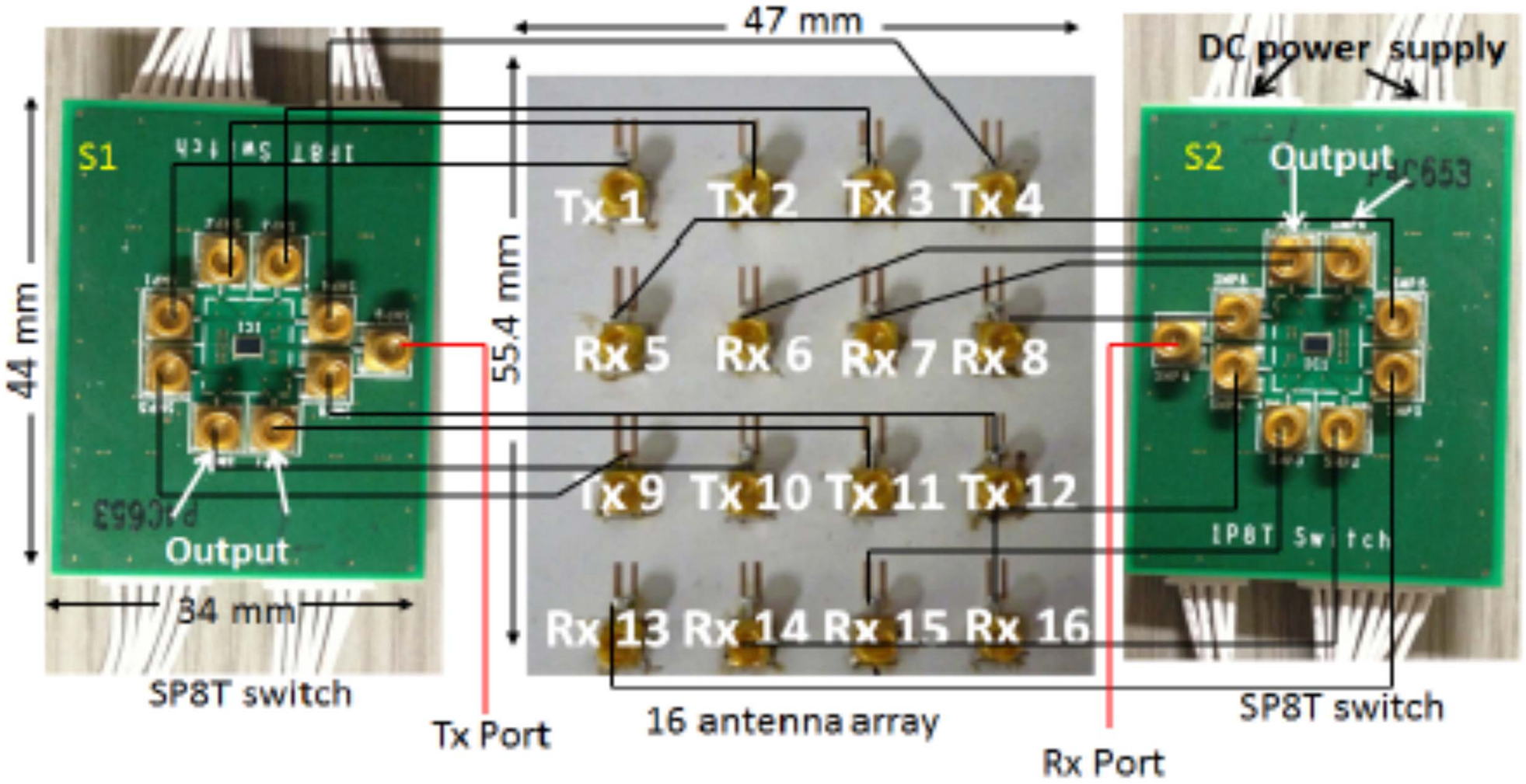

A. Azhariet *et al*., Proc. IEEE Biomedical Circuits and Systems Conference, 22-24 Oct. 2014,

SP8T Switching Matrix

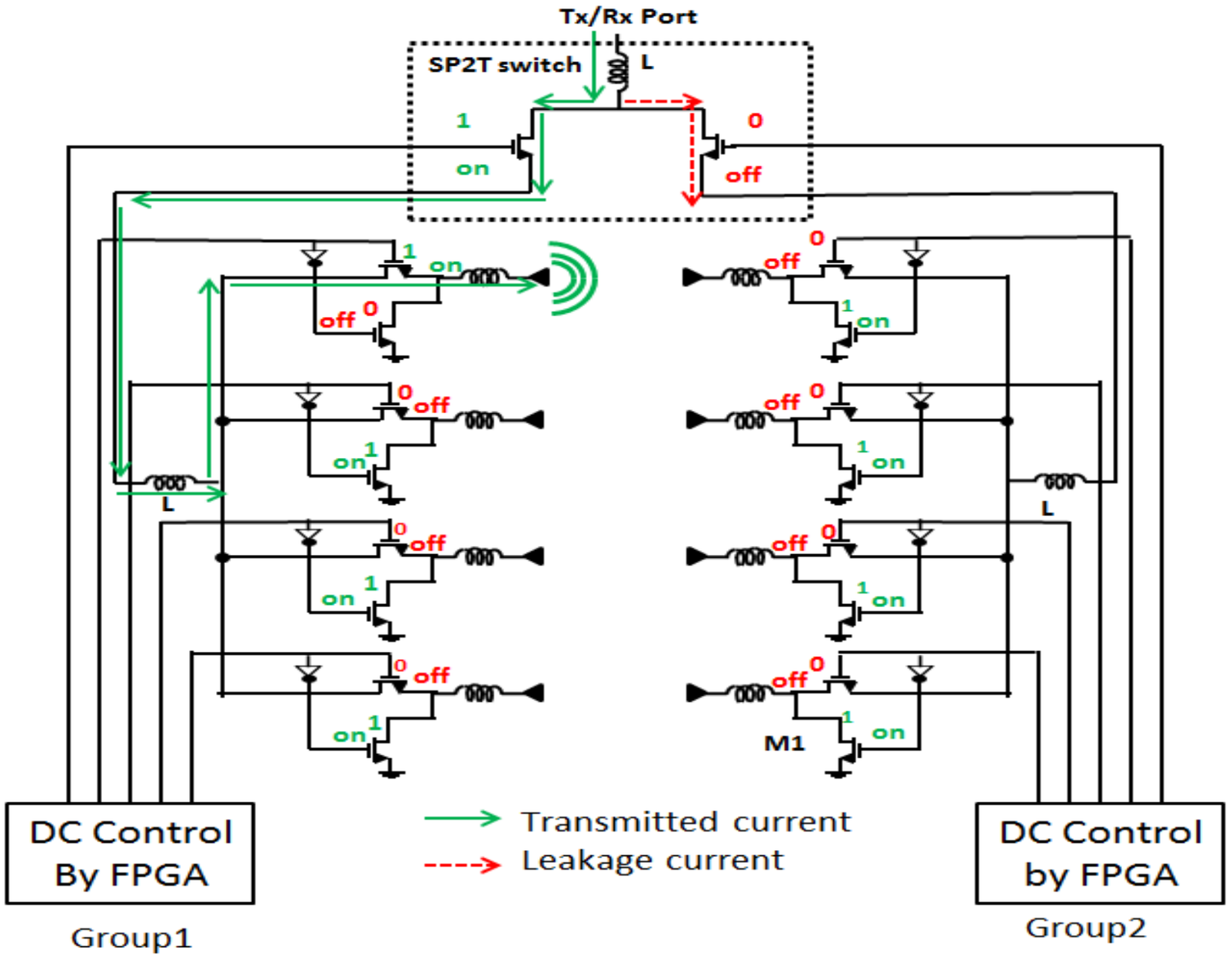

A. Azhariet *et al*., Proc. IEEE Biomedical Circuits and Systems Conference, 22-24 Oct. 2014,

UWB Antenna

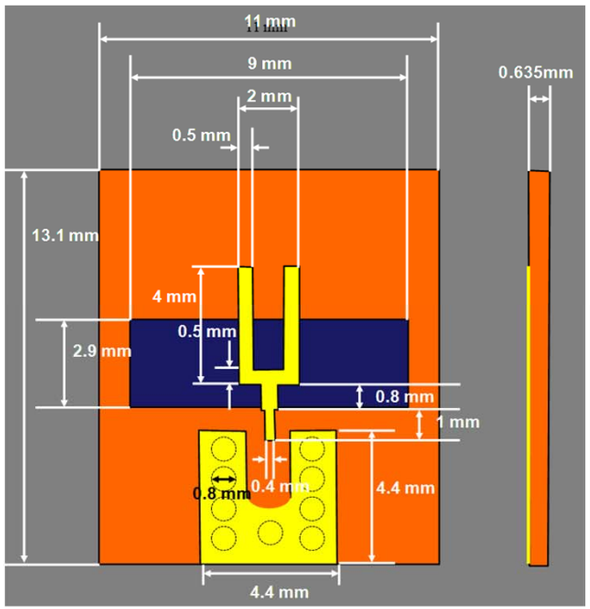

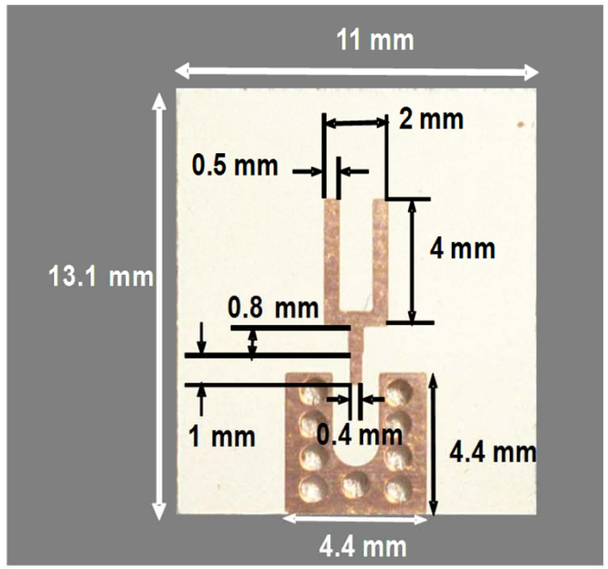

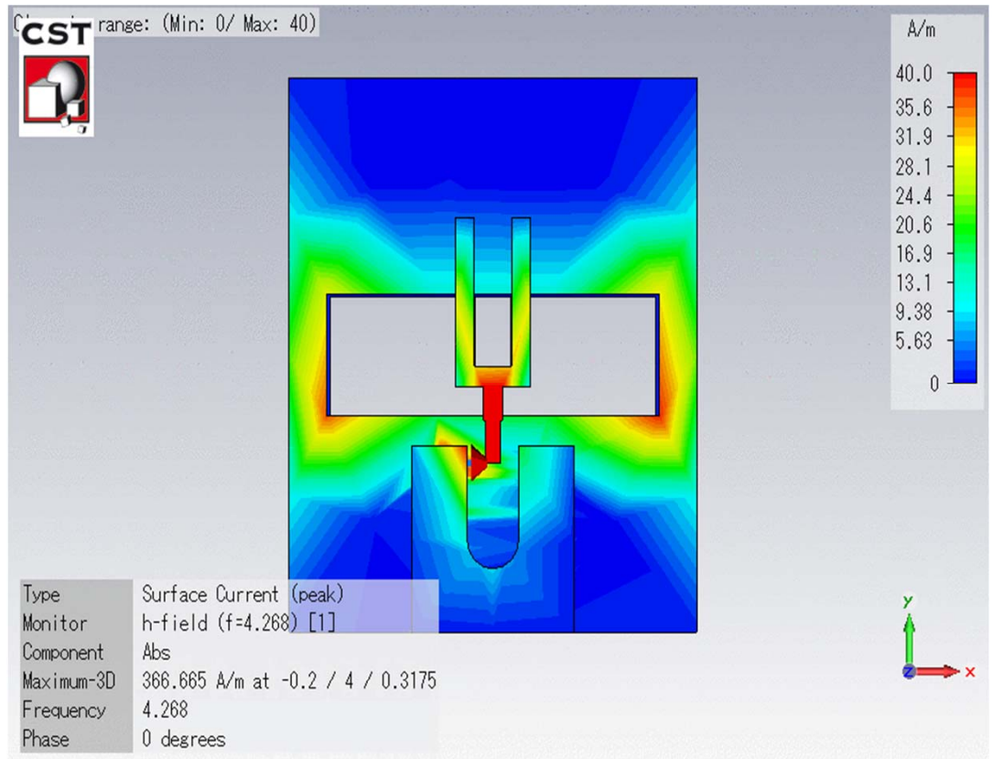

H. Song *et al*., Scientific Reports volume 7, Article number: 16353 (2017)

4x4 UWB Antenna Array

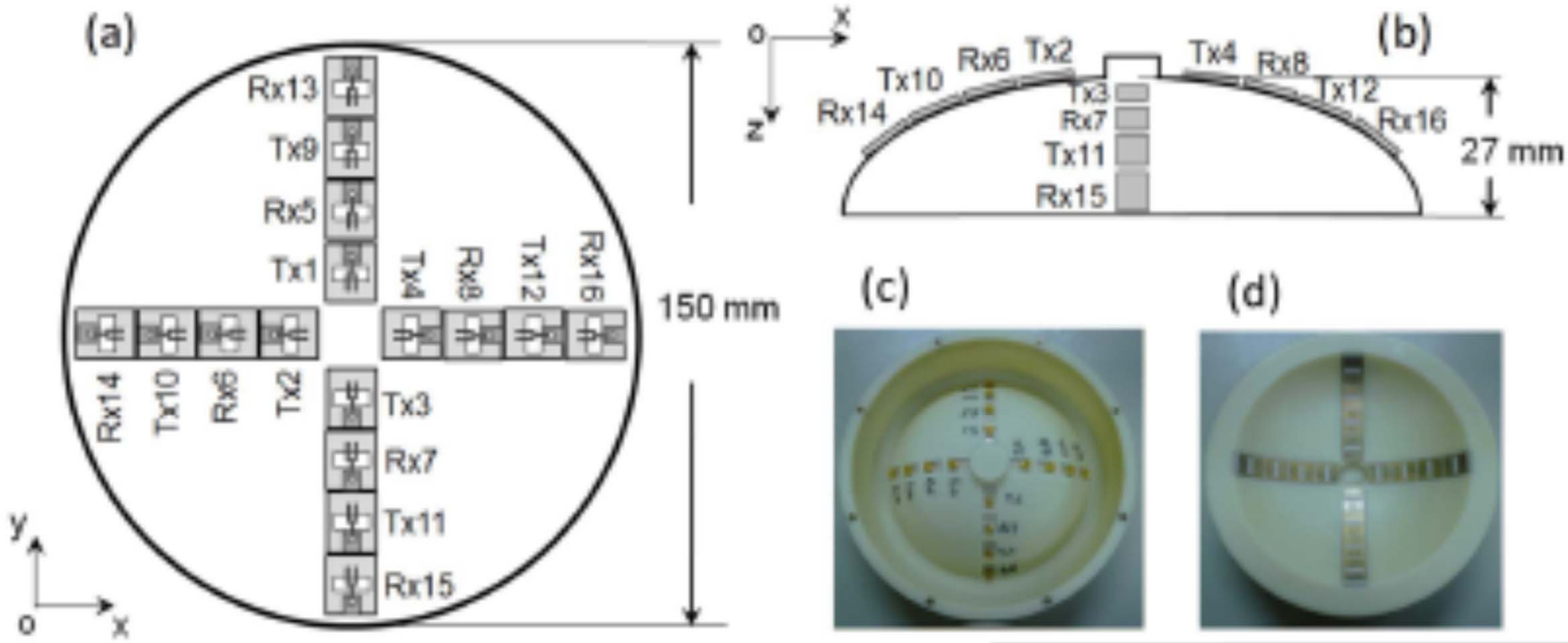

H. Song *et al*., Scientific Reports volume 7, Article number: 16353 (2017)

Hand-held Impulse-Radar Detector

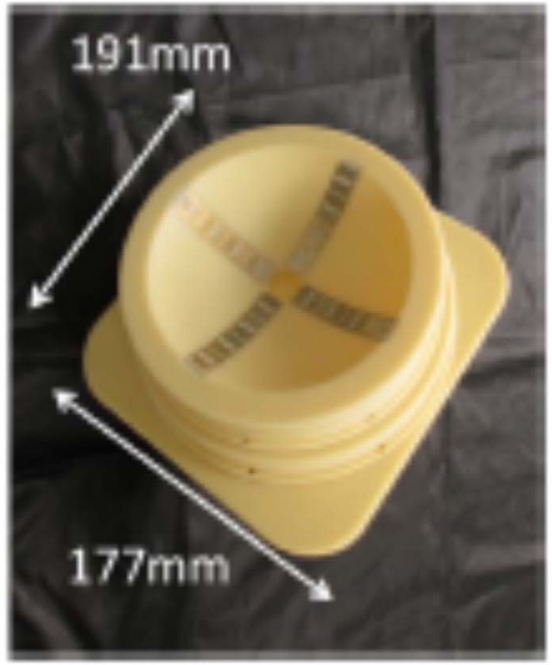

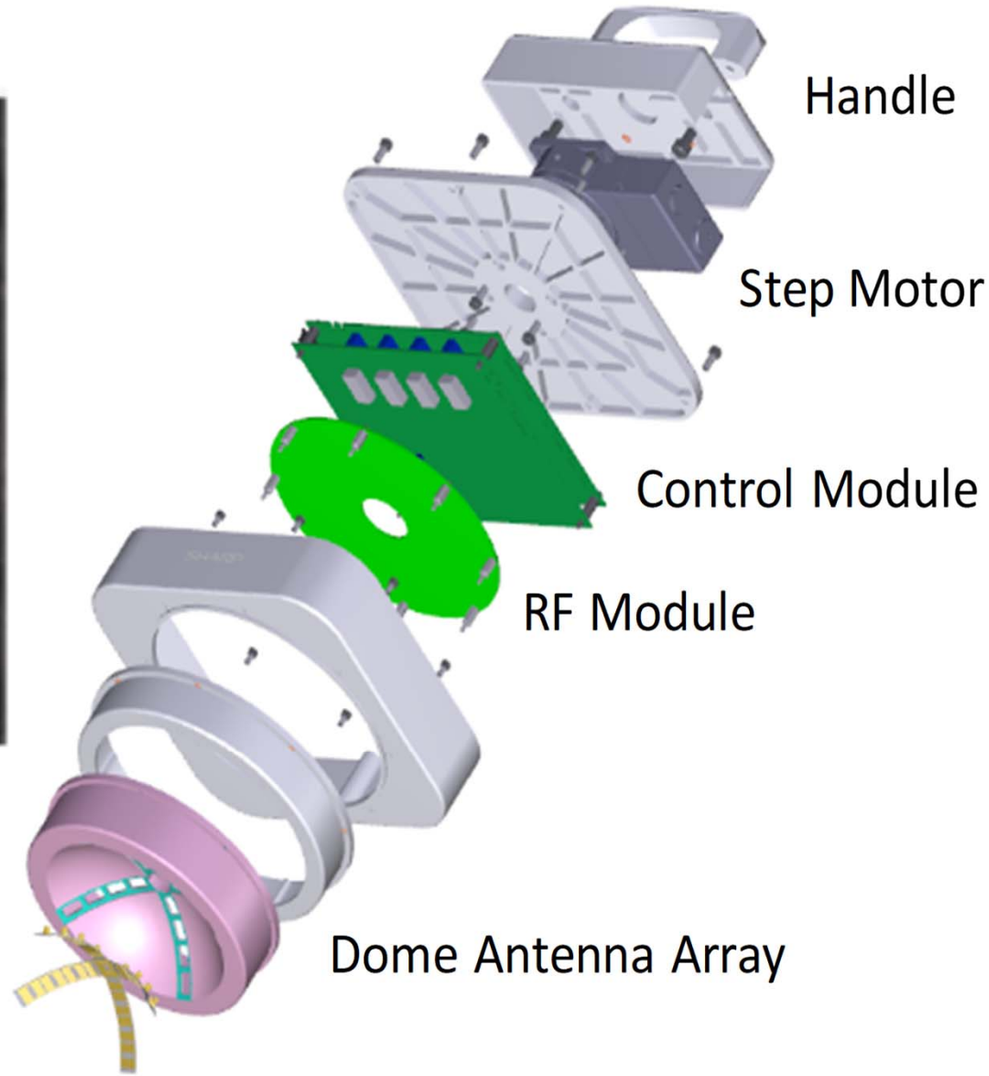

H. Song *et al*., Scientific Reports volume 7, Article number: 16353 (2017)

Hand-held Impulse-Radar Detector

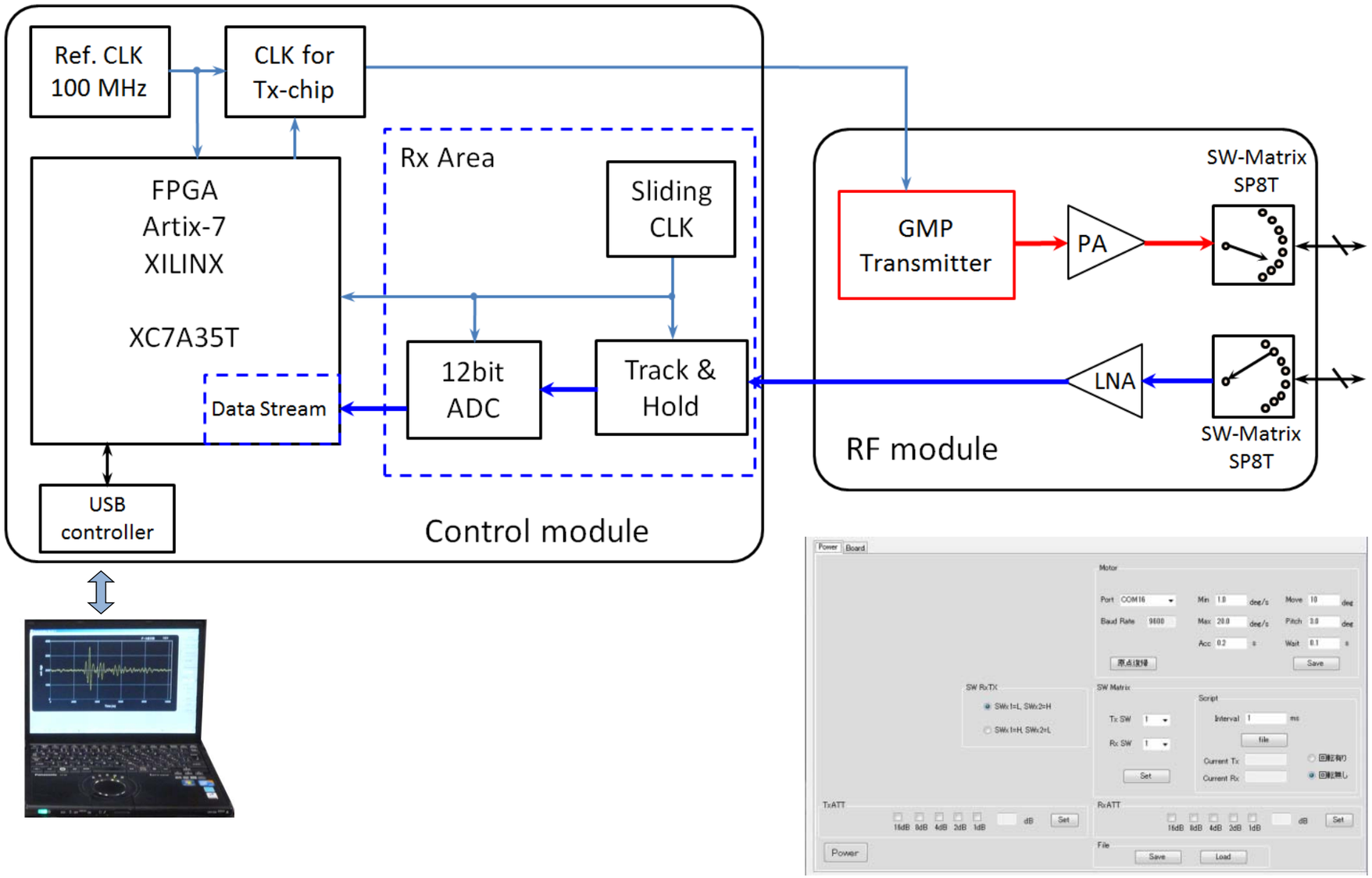

H. Song *et al.*, Scientific Reports volume 7, Article number: 16353 (2017)

Impulse-Radar Detector RF Module

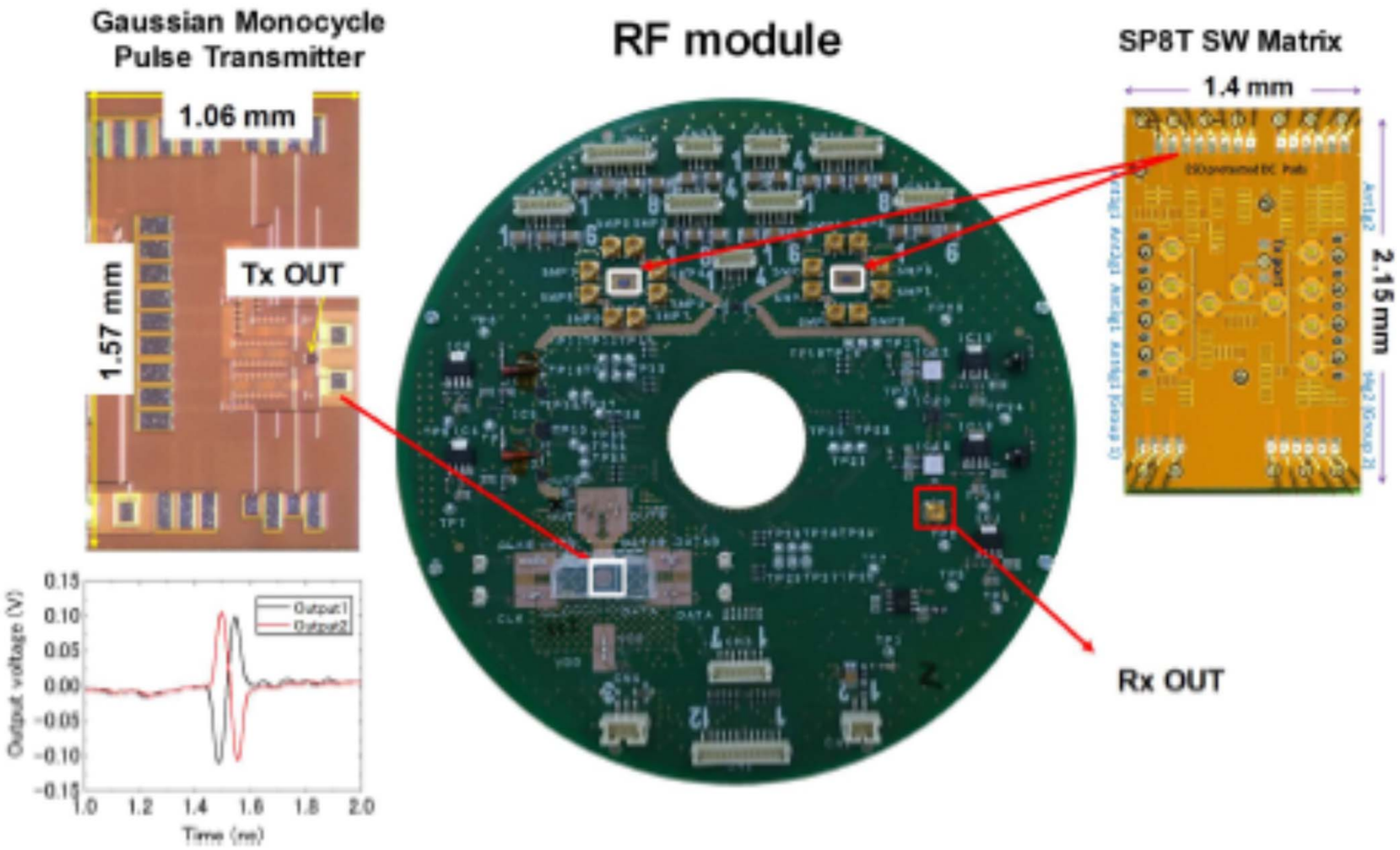

H. Song *et al.*, Scientific Reports, vol. 7, Article number: 16353 (2017)

Level Diagram of Impulse-Radar Detector

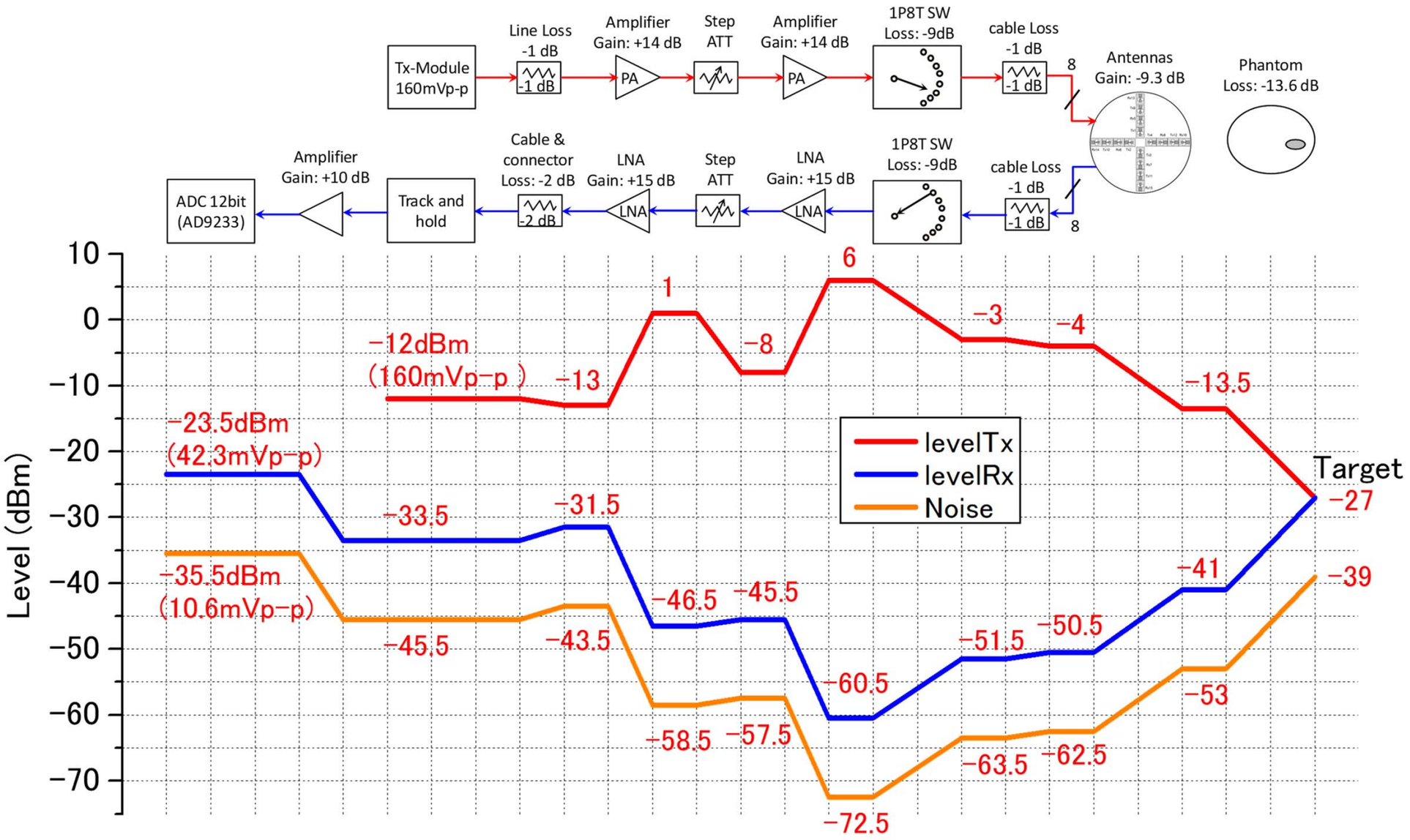

H. Song *et al*., Scientific Reports, vol. 7, Article number: 16353 (2017)

Detectability of Tumor Phantom

- Detector rotates clockwise around antenna center, signals obtained from 120 angles
- 1-cm^3 bacon target is inserted into the phantom (dielectric constant is 45 at 6 GHz)
- Peak of received signals after A/D conversion is 2300 LSB (least significant bit) corresponding to 12-bit ADC

Breast Phantom: Silicone
Tumor Phantom: Bacon

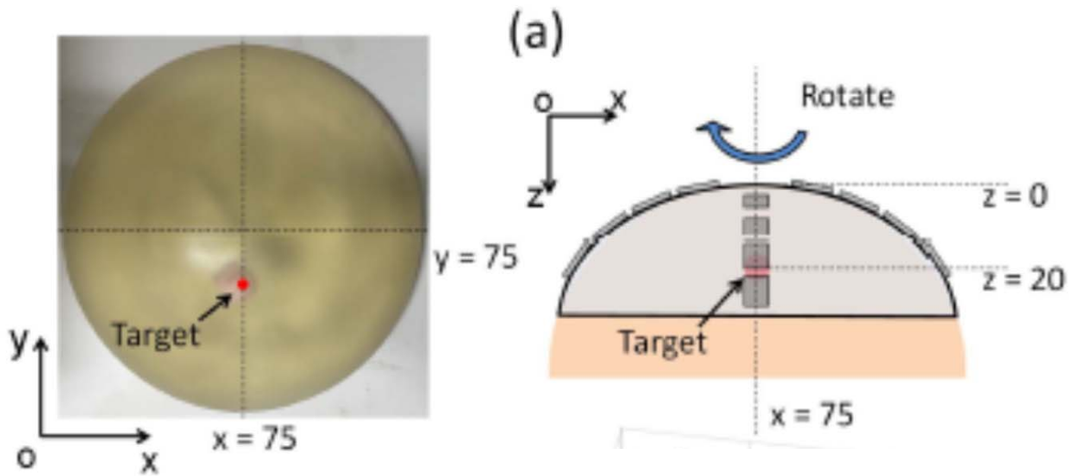

Received Signals vs. rotation angle

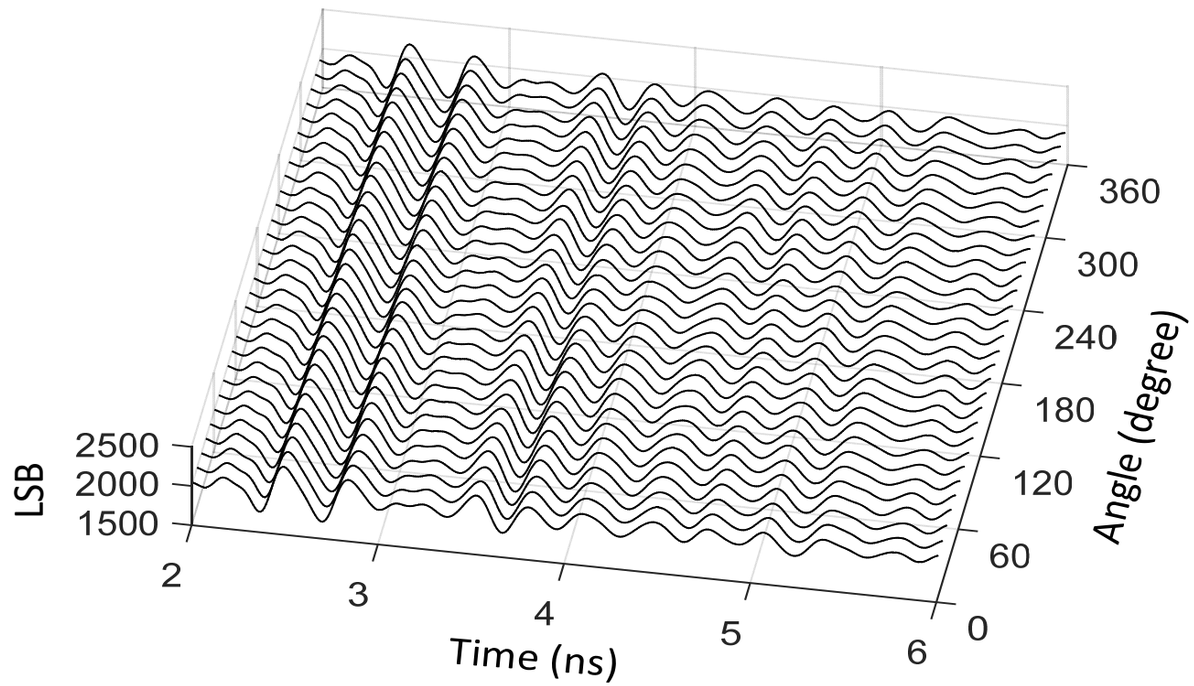

H. Song *et al*., Scientific Reports, vol. 7, Article number: 16353 (2017)

Detectability of Tumor Phantom

- Scattered signals very weak compared with direct wave, cannot be observed explicitly in raw form
- Reference signal formed by averaging all received signals to eliminate scattered signals from the target which arrive at different times → extract target reflections after subtracting reference signal
- Subtracted waveforms for 0–360° rotation (120 angles) are shown
- Amplitude is 100 LSB after A/D conversion due to the loss in the phantom
- Reconstruct breast image after applying confocal algorithm to subtracted signals

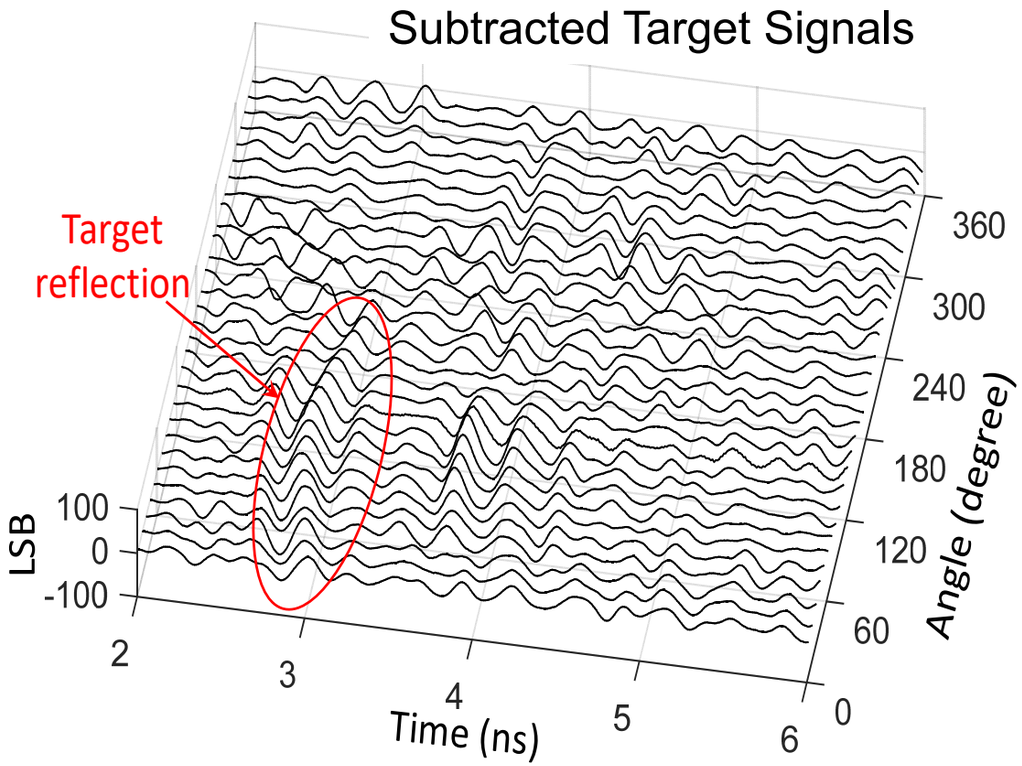

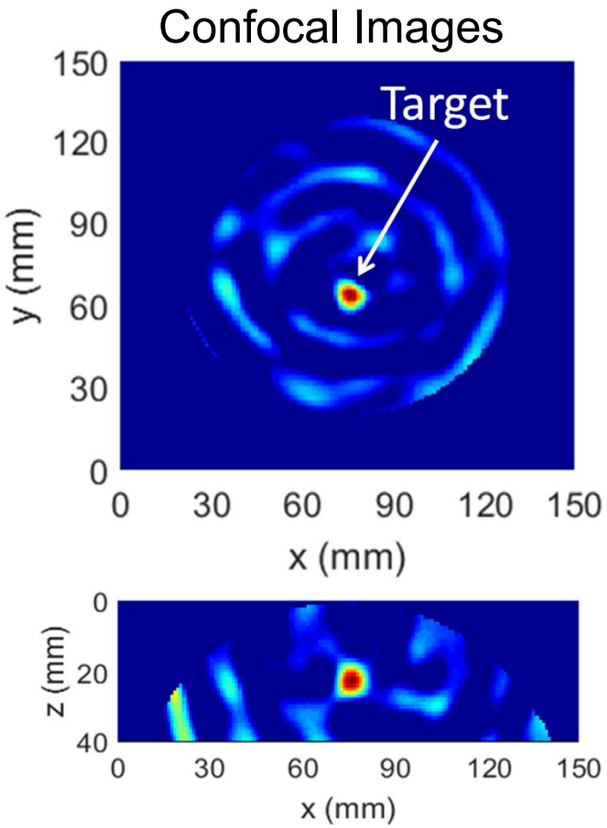

H. Song *et al*., Scientific Reports, vol. 7, Article number: 16353 (2017)

Detectability of Excised Tumor Tissue

- System applied to excised breast tissues after total mastectomy surgery at Hiroshima University Hospital
- After operation, breast is first dissected by pathologist to confirm tumor position and take tumor samples for diagnosis
- Breast is covered with poly-ethylene film to isolate blood and fold the cut incision
- Impulse-radar-detector is placed on breast tissue for imaging

Excised Tumor Tissue

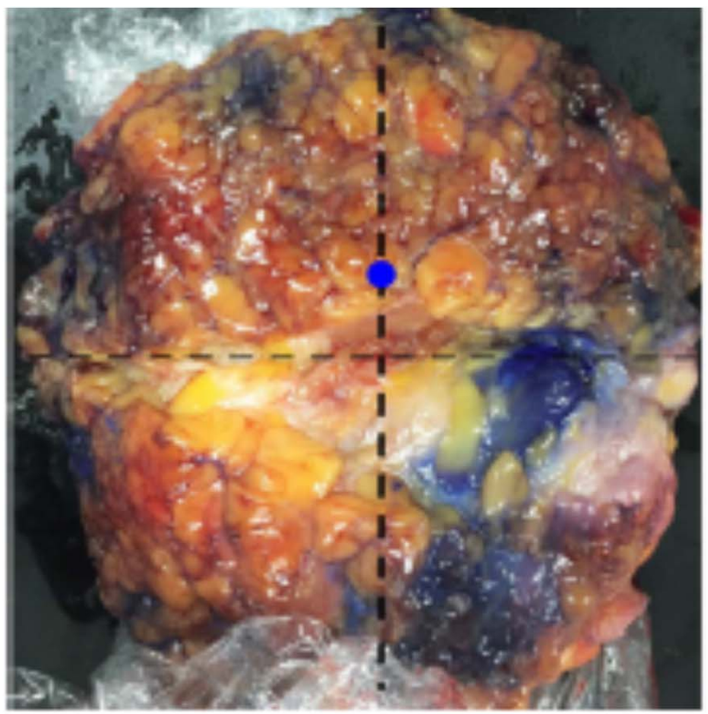

Impulse Radar Detector

H. Song *et al*., Scientific Reports, vol. 7, Article number: 16353 (2017)

Confocal Images of Excised Tumor Tissue

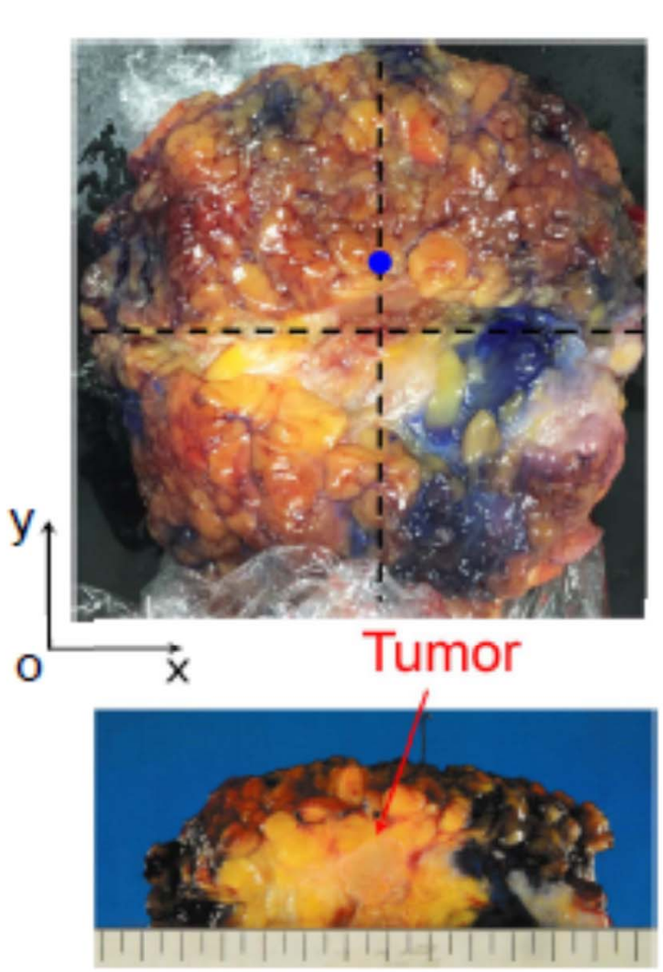

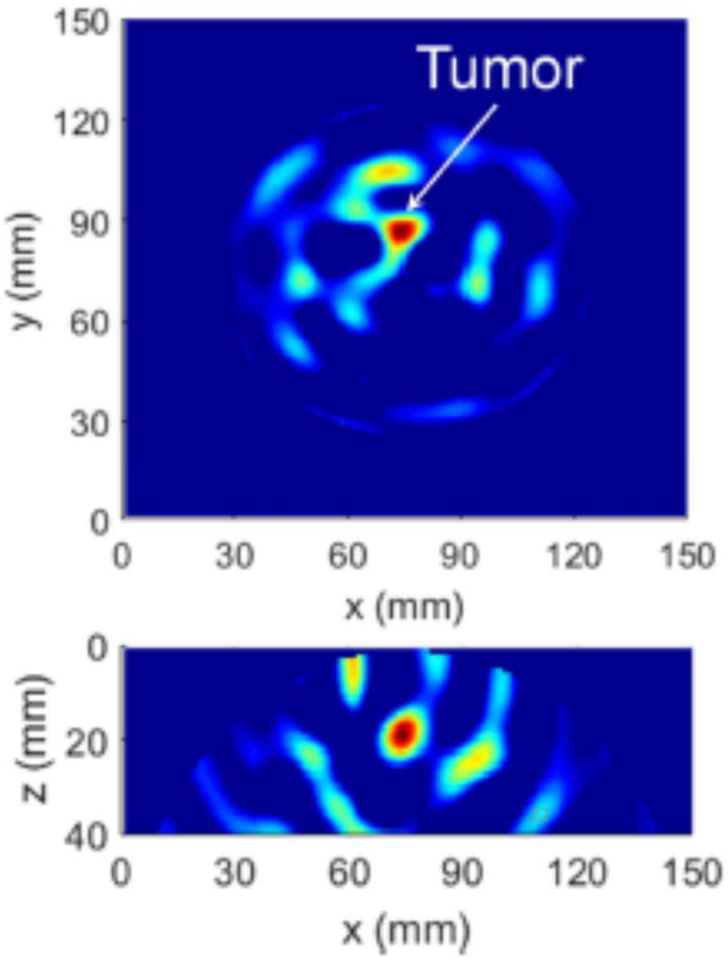

Coronal

Sagittal

H. Song *et al*., Scientific Reports, vol. 7, Article number: 16353 (2017)

Clinical Examination

Pilot clinical test

- In clinical applications, five volunteer patients, who have been diagnosed with breast cancer, were recruited with ethical approval and informed consent. Malignant tumors include invasive ductal carcinoma (IDC) and ductal carcinoma *in situ* (DCIS).

- Patients were informed of the total process and signed consent. Before the test, the clinical doctors were trained to use the detector. The clinical tests were conducted at the Hiroshima University Hospital by the oncologists without any engineers present.

- By comparing the imaging results with the MRI, X-ray and PET (positron emission tomography), the conclusion was made.

Clinical Examination

Ethical approval and informed consent:

- Performed pilot clinical tests conducted by following guidelines and protocols of the Japan Clinical Oncology Group protocol manual ver.2.6, which approved the breast cancer detector and its measurement procedure (Hiroshima University Clearance number: C-153)
- UMIN-CTR (University Hospital Medical Information Network-Clinical Trials Registry) number is UMIN000026181. Informed consents of all volunteers obtained before the clinical test.

Table 1 Patient characteristics.

					Tumor size (cm)								
Case	Age (y)	Tumor side	Tumor location	Histology	Pathological invasive size	MMG	US	MRI	PET	ER	PgR	HER2	Ki-67 (%)
1	67	Left	Upper-inner	IC-NST	2.5	2.3	2.1	2.1	1.6	+	+	+	13
2	43	Right	Upper-outer	IC-NST	1.1	–	2.6	1.5	1.4	+	+	+	20
3	73	Left	Upper-inner	Microinvasive	0.05	3.4	3.6	2.6	3.3	+	+	–	17
4	58	Left	Central	IC-NST	2.8	2.6	2.1	2.8	2.5	+	+	+	20
5	36	Left	Upper-inner	IC-NST	2.5	1.9	1.9	2	1.4	+	+	–	47

Note: ER, estrogen receptor; HER2, human epidermal growth factor receptor 2; IC-NST, invasive carcinoma of no special type; MMG, mammography; MRI, magnetic resonance imaging; PET, positron emission tomography; PgR, progesterone receptor; SUV, standardized uptake value; US, ultrasonography.

S. Sasada et al., *J. Med. Imag.* 5(2), 025502 (2018),

32

Clinical Examination

- Patients laid down in supine position and detector is placed on breast
- Green marker is pasted on the outside of the system, indicating start angle position pointing to the head; rotation is clockwise
- x-axis set on intersection of transverse and coronal planes
- y-axis set on intersection of sagittal and coronal planes

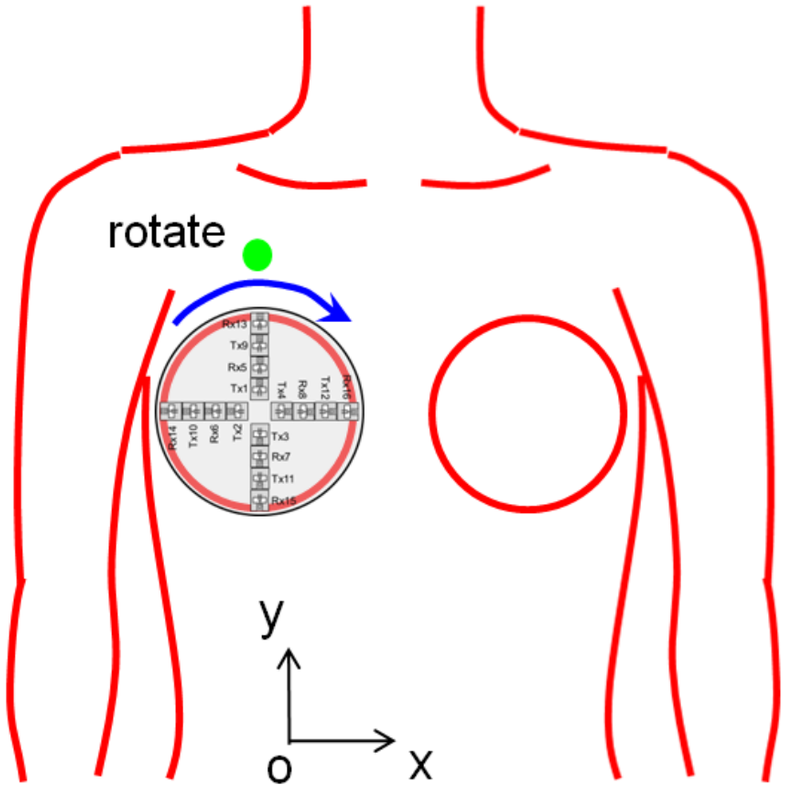

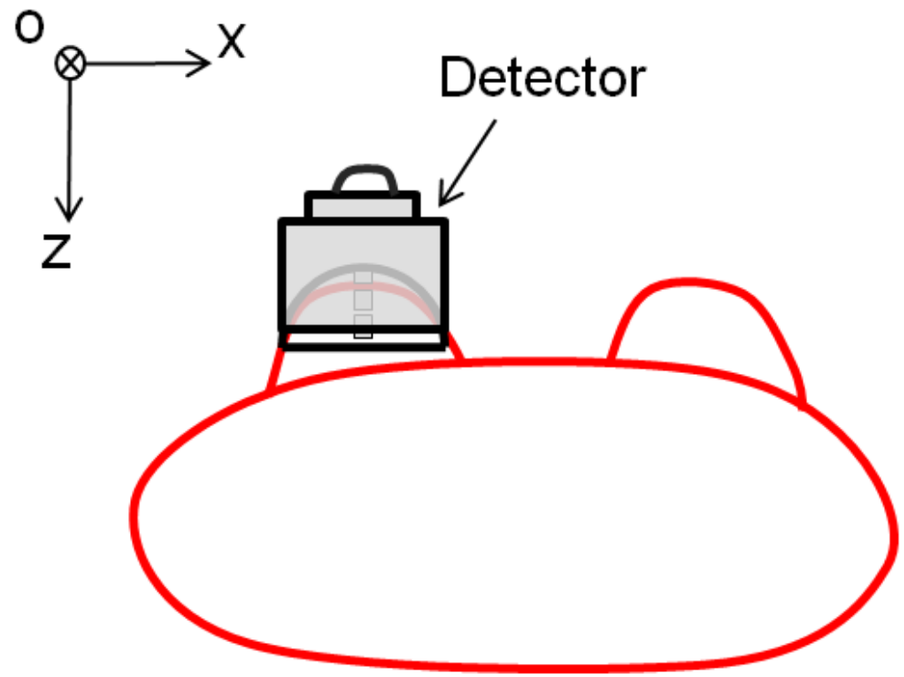

H. Song *et al*., Scientific Reports, vol. 7: 16353 (2017)

Clinical Examination

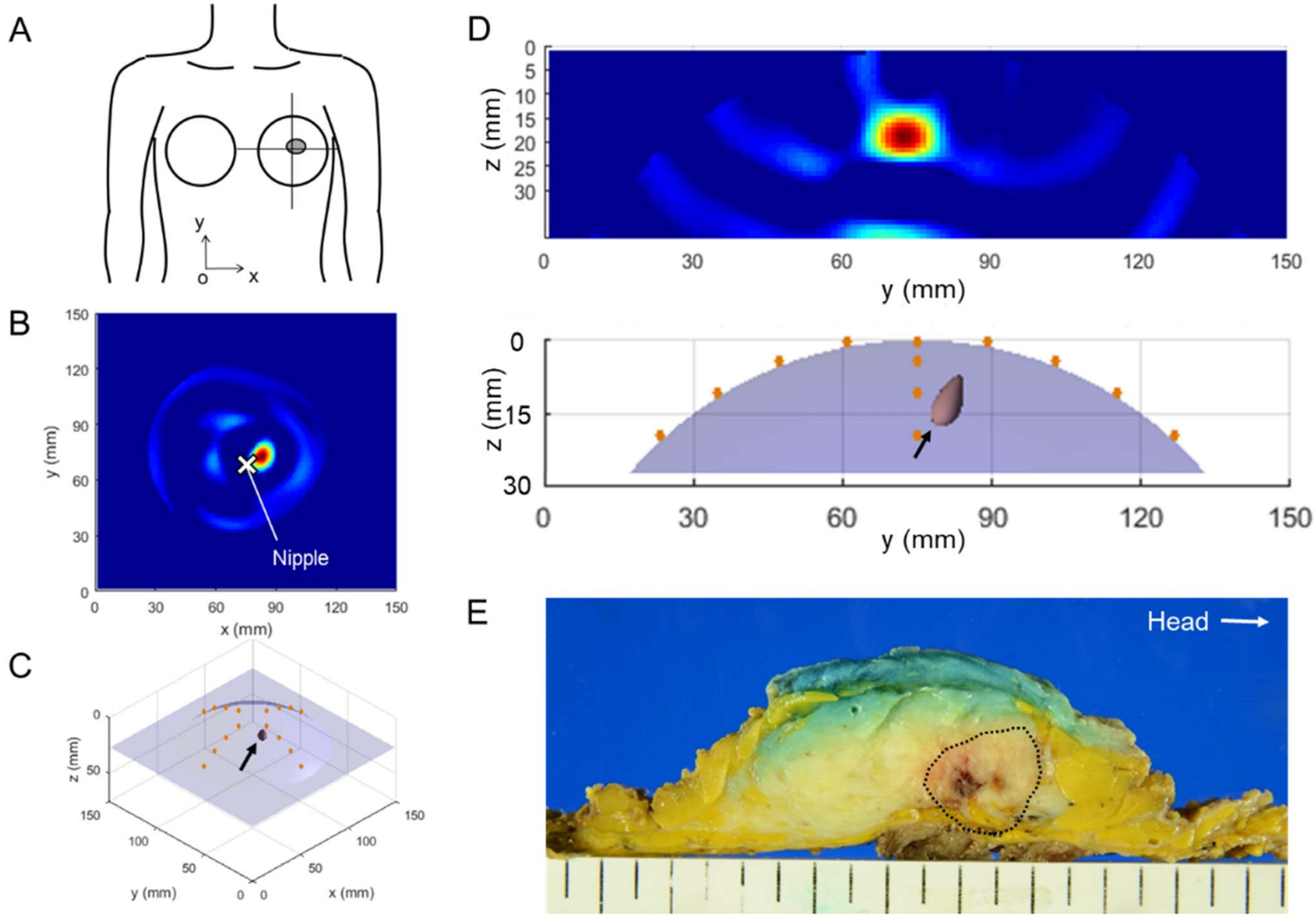

S. Sasada *et al*., *J. Med. Imag.* 5(2), 025502 (2018),

Clinical Examination

Confocal Images

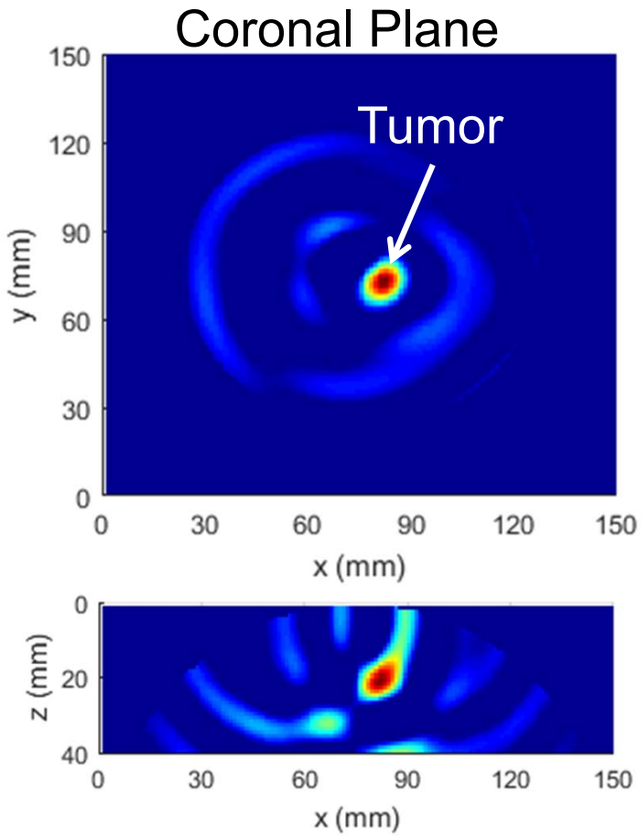

3-D Position of Patient's Cancer

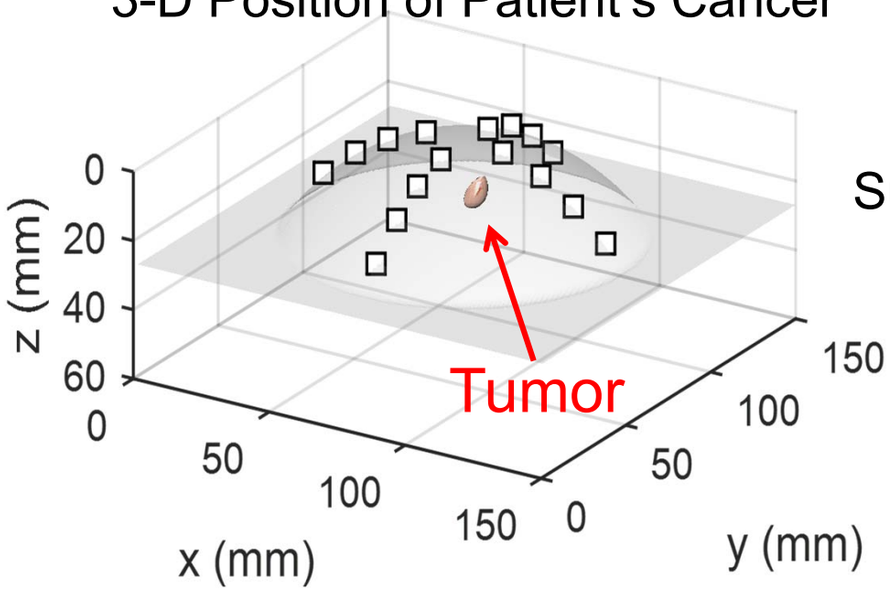

Supine

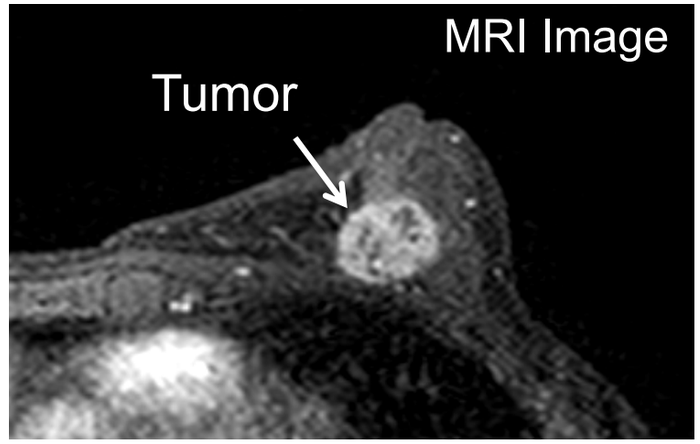

Prone

H. Song, et al., Scientific Reports, vol. 7, Article number: 16353 (2017)

Clinical Examination Case 1

Malignant tumor can be detected by the impulse-radar-based detector.

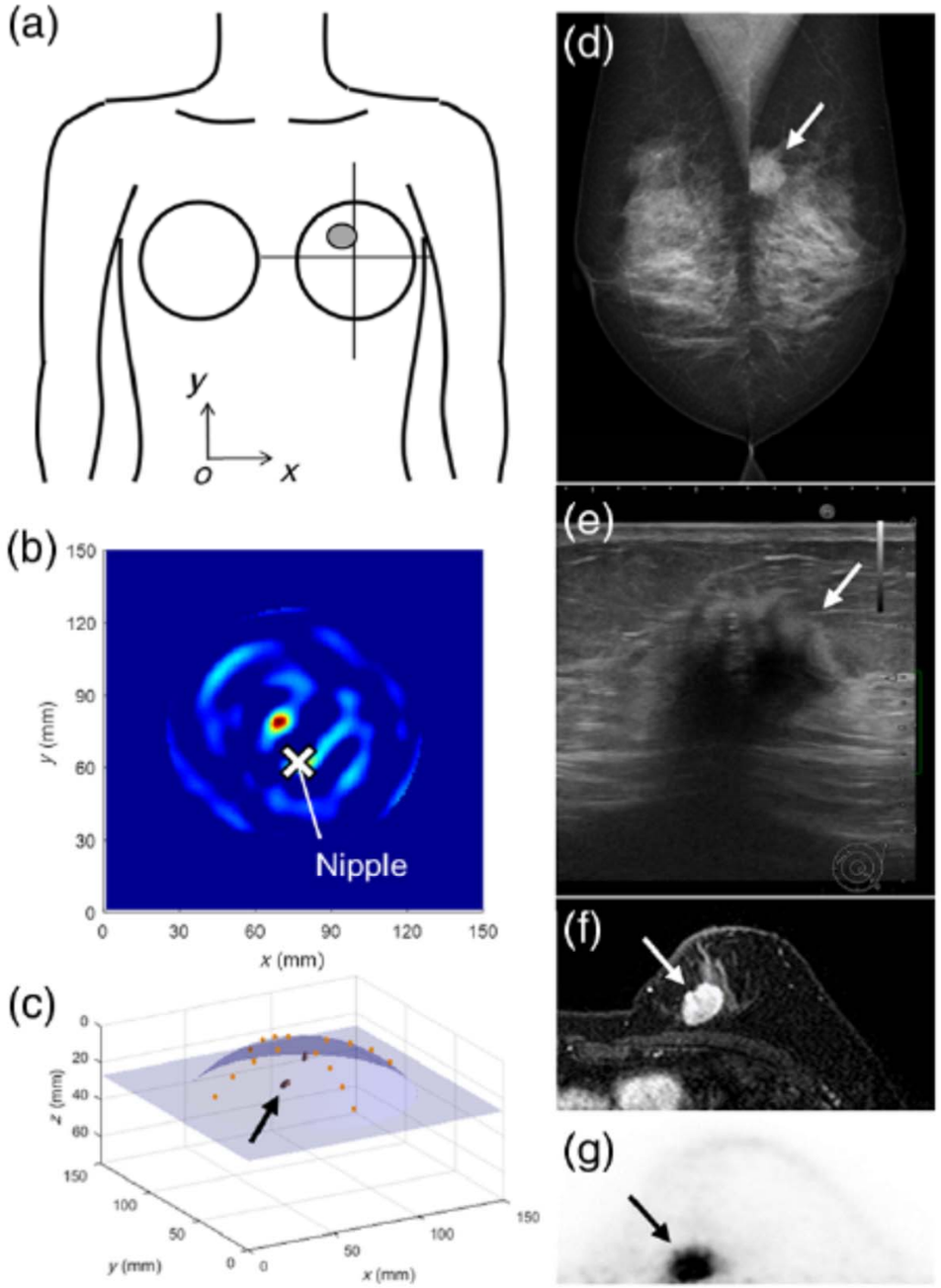

X-ray

Ultrasound

MRI

PET

S. Sasada *et al*., *J. Med. Imag.* 5(2), 025502 (2018),

Clinical Examination Case 2

X-ray mammography failed to detect the cancer because of dense breast of a young patient, whereas impulse-radar-based detector can detect the cancer successfully.

This system has a potential for early stage cancer screening for young women without pain and ionizing radiation.

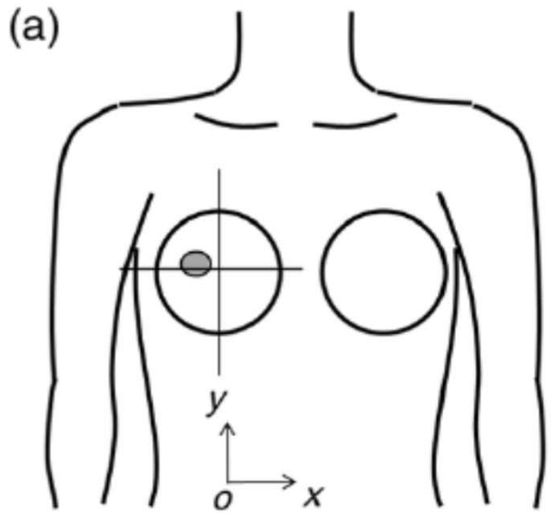

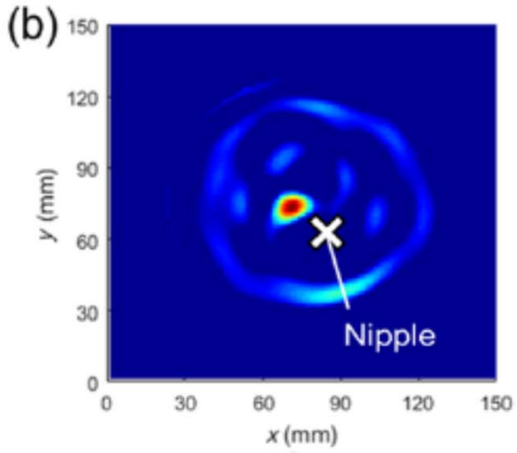

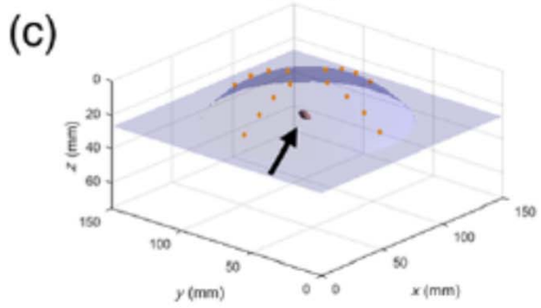

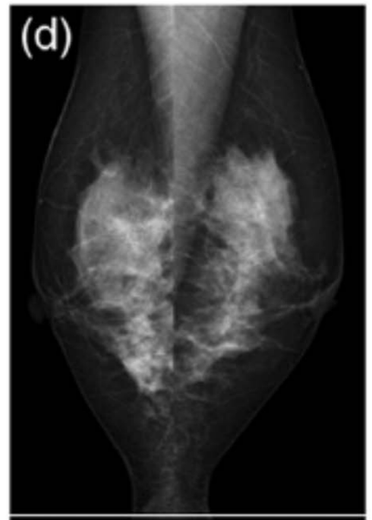

X-ray

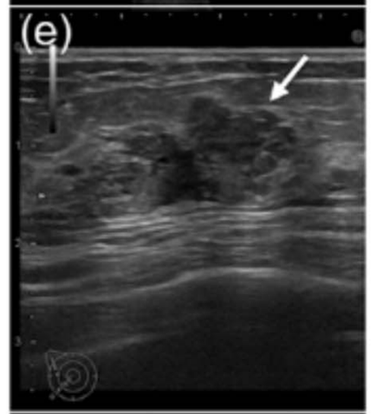

Ultrasound

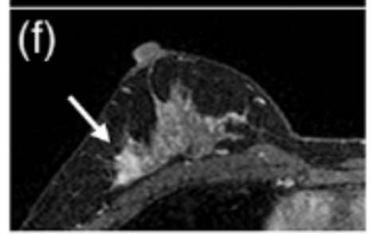

MRI

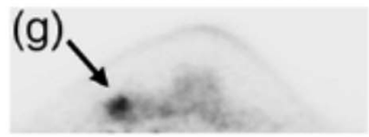

PET

S. Sasada *et al.*, *J. Med. Imag.* 5(2), 025502 (2018),

Clinical Examination Case 3

Micro-invasive cancer with 0.05mm size can be detected by impulse-radar-based detector.

Early stage cancer with extensive intra-ductal component (EIC) can be detected by impulse-radar-based detector.

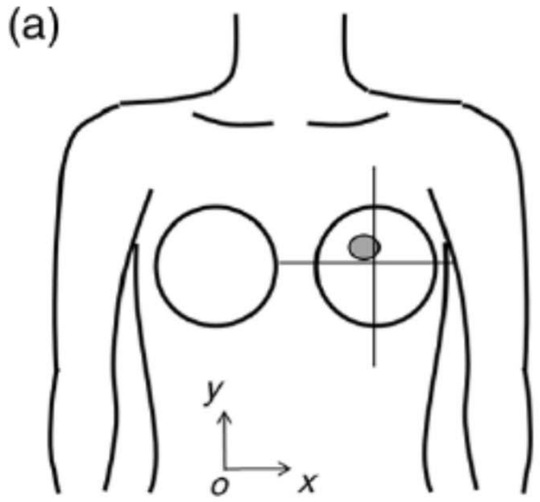

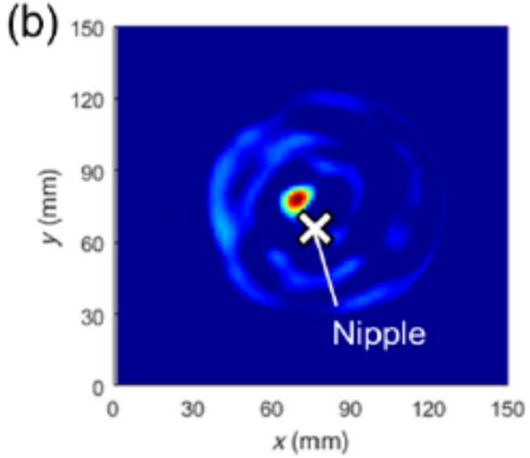

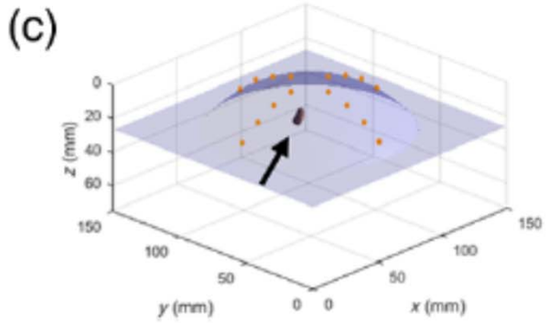

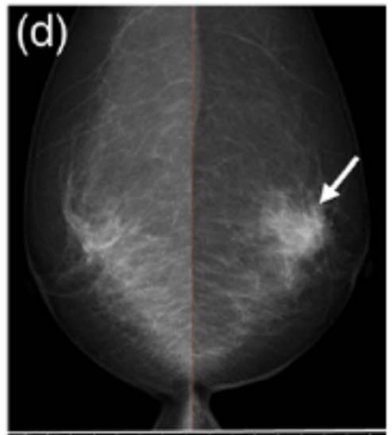

X-ray

Ultrasound

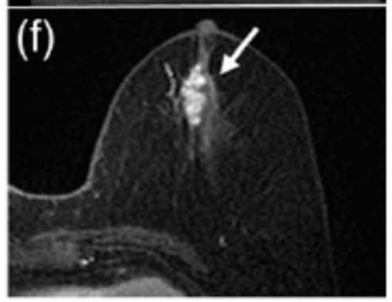

MRI

PET

S. Sasada *et al*., *J. Med. Imag.* 5(2), 025502 (2018),

Conclusion

- Hand-held impulse-radar breast cancer detector was developed using CMOS ICs for the first time.
- 100% detectability of malignant breast tumors was demonstrated in the clinical test at Hiroshima University Hospital.
- Confocal imaging results are consistent with those of MRI and PET, demonstrating the feasibility of the hand-held impulse-radar detector for malignant breast tumors.
- Impulse-radar-based detector has potential for early stage cancer screening for young women without pain and ionizing radiation.